FACULTY
OF MECHANICAL
ENGINEERING
CTU IN PRAGUE

Department of Designing and Machine Components

Design of a Composite Beam Pipe for CBM Experiment

MASTER'S THESIS

2021

Bc. Martin SMETANA

Study programme:	(NDTT) Automotive, Railway and Transportation Engineering
Specialization:	(N071TTTE) Transportation Engineering

ZADÁNÍ DIPLOMOVÉ PRÁCE

I. OSOBNÍ A STUDIJNÍ ÚDAJE

Příjmení: **Smetana** Jméno: **Martin** Osobní číslo: **457567**

Fakulta/ústav: **Fakulta strojní**

Zadávající katedra/ústav: **Ústav konstruování a částí strojů**

Studijní program: **Dopravní a transportní technika**

Specializace: **Transportní technika**

II. ÚDAJE K DIPLOMOVÉ PRÁCI

Název diplomové práce:

Návrh kompozitového iontovodu pro experiment CBM

Název diplomové práce anglicky:

Design of a Composite Beam Pipe for CBM Experiment

Pokyny pro vypracování:

Navrhněte kompozitový iontovod pro experiment CBM pro urychlovač FAIR v GSI Darmstadt v Německu. Iontovot bude na jedné straně napojen na naklápěcí mechanismus, na druhé straně bude ukončen víčkem. Průměr trubky je maximálně 200mm. Celková délka iontovodu je 12m. Trubka bude složená z několiko modulů. Maximální délka modulu je omezena na 5m. Navrhněte vhodné kontrukční řešení spojení s naklápecím mechanismem a mezi jednotlivými moduly. Navrhněte vhodný počet a umistění vstupů pro odsávání vakua (1e-3mbar). Navrhněte podpůrnou kontrukci pro iontovod, který bude vedený ve výšce 5m nad zemí. Proveďte MKP výpočet iontovodu zatížený vnějším přetlakem a vlastní hmotností, zpracujte výsledky provedeného experimentu a porvnejte je s provedeným MKP výpočtem.

Seznam doporučené literatury:

Jméno a pracoviště vedoucí(ho) diplomové práce:

Ing. Martin Janda, ústav konstruování a částí strojů FS

Jméno a pracoviště druhé(ho) vedoucí(ho) nebo konzultanta(ky) diplomové práce:

Datum zadání diplomové práce: **12.04.2021** Termín odevzdání diplomové práce: **04.06.2021**

Platnost zadání diplomové práce: _____

Ing. Martin Janda	Ing. František Lopot, Ph.D.	prof. Ing. Michael Valášek, DrSc.
podpis vedoucí(ho) práce	podpis vedoucí(ho) ústavu/katedry	podpis děkana(ky)

III. PŘEVZETÍ ZADÁNÍ

Diplomant bere na vědomí, že je povinen vypracovat diplomovou práci samostatně, bez cizí pomoci, s výjimkou poskytnutých konzultací. Seznam použité literatury, jiných pramenů a jmen konzultantů je třeba uvést v diplomové práci.

30.4.2021
Datum převzetí zadání

Podpis studenta

INSTRUCTIONS FOR DIPLOMA THESIS

Design a composite Beam Pipe for the CBM experiment for the FAIR accelerator at GSI Darmstadt in Germany. The pipe is connected to the tilting mechanism on one side and is determined by a lid on the other side. The diameter of pipe is 12 m. The tube must consists of several modules. The maximum length of the module is limited to 5 m. Design a suitable design solution for the connection with the tilting mechanism and between the individual modules. Design a suitable number and location of inlets for vacuum extraction (1e-3 mbar). Design a supporting structure for the pipe, which is run at a height of 5 m above the ground. Perform an FEM calculation of the pipe loaded with external overpressure and its own weight, process the results of the performed experiment and compare them with the performed FEM calculation.

Acknowledgements

I would like to take this opportunity to sincerely thank the supervisor of this thesis, Martin Janda, for his professional supervision, assistance, and overall support during the completion of this work. I would also like to thank Martin Rachač and Petr Chudoba, for their valued help in providing priceless professional insight. Finally, I would like to thank the employees of the Czech Technical University, who helped with the preparation of materials, samples, and equipment for this work.

SWORN STATEMENT

I declare that I have worked on this diploma thesis titled "Design of a Composite Beam Pipe for a CBM experiment" alone, under the supervision of Ing. Martin Janda. All of the information sources used are listed at the end of the thesis. The citation of literature follows the standard ISO 690.

Prague, July 30th 2021 Martin Smetana

ANNOTATION LIST

Name of author: *Martin SMETANA*

Title in English: *Design of a Composite Beam Pipe for CBM experiment*

Title in Czech: *Návrh kompozitového iontovodu pro experiment CBM*

Year: *2021*

Field of study: (N071TTTE) Transportation Engineering

Department: *Department of designing and machine elements*

Supervisor: *Ing. Martin JANDA*

Tutor: *Ing. Marek RACHAČ*

Bibliographic information:

number of pages	66
number of figures	76
number of tables	5
number of attachments	8

Keywords in English: Beam Pipe, compressed baryonic matter, composite, vacuum

Keywords in Czech: iontovod, stlačená baryonová hmota, kompozit, vakuum

ABSTRACT IN ENGLISH:

This thesis is focused on the construction design of a composite Beam Pipe consists of several modules. The thesis contains a few possible design of modules connections, supports of Beam Pipe and a cap to close it. FEM analysis were performed for individual types of connections. CAD models of all parts of the Beam Pipe were created. An experiment was performed, its processing and a model for FEM was created.

ABSTRACT IN CZECH:

Tato diplomová práce je zaměřena na konstrukční návrh kompozitového iontovodu modulového provedení. Práce obsahuje několik možných řešení spojování modulů, podpěr celého iontovodu a jeho uzavření. Na jednotlivé druhy spojení byly provedeny MKP analýzy. Byly vytvořeny CAD modely všech částí iontovodu. Byl proveden experiment, jeho zpracování a vytvořen model pro MKP.

TABLE OF CONTENTS

1. Introduction 3
2. Composite material 5
2.1. History of composite material 5
2.2. Composite manufacturing techniques 6
2.2.1. Open contact moulding 6
2.2.2. Resin infusion processes 7
2.2.3. Compression moulding 7
2.2.4. Pultrusion process 8
2.2.5. Filament winding 9
3. Vacuum 11
3.1. Vacuum categories according to vacuum quality 11
3.2. Vacuum pumps categories according to principle 11
3.3. Vacuum pumps categories according to vacuum quality 12
3.4. Scroll pump 13
3.5. Turbomolecular pump 13
3.6. Vacuum Connections 14
3.6.1. Non-detachable connections 14
3.6.2. Detachable connections 15
3.6.2.1. ISO-KF flange 15
3.6.2.2. ISO-K flange 16
3.6.2.3. ISO-F flange 16
3.6.2.4. ISO-CF flange 17
3.7. Vacuum conductance 18
3.8. Pressure profile 18
3.9. Gas release from solids 19
3.10. Numerical method for calculating pressure profile 21
3.11. Vacuum calculation 22
4. O-rings 25
4.1. Dimensions of groove for O-rings 26
5. Design 29
5.1. Determining Beam Pipe basic dimensions 29
5.1.1. Length of the Beam Pipe 29
5.1.2. Diameter of the Beam Pipe 30
5.1.3. Wall thickness 31
5.2. Connections 34
5.2.1. Slide-in connection 34
5.2.2. Flange connection 35
5.2.3. FEM Analysis of connections 38
5.3. Modules 40
5.4. Vacuum inputs 44
5.5. Supports 45
5.6. PSD passage 50

5.6.1. FEM analysis 51
5.7. Beam Pipe 53
6. Experiment 55
7. Conclusion 59
8. REFERENCE....62
LIST OF FIGURES 65
LIST OF TABLES 66
LIST OF ATTACHMENTS 66

1. Introduction

This Master's thesis is focused on the design of composite Beam Pipe. The Beam Pipe is basically a simple long pipe that will be loaded by its own weight and overpressure. Its overall composition from the modules needs to be resolved, as producing it at the required length would be very costly, if not impossible. The tube will be able to tilt ±2.5°, so the definition of motion needs to be resolved in relation to the tilting mechanism. There will be a vacuum inside and there is a need to clarify the number of inputs and where it will be appropriate to place them, so that the required value is not exceeded. After designing the key components, it will be necessary to check that they are not overly stressed before making the component. This will be done by FEM analysis, which will be applied to the key elements.

The Compressed Baryonic Matter (CBM) experiment will be one of the major scientific pillars of the future Facility for Antiproton and Ion Research (FAIR) in Darmstadt. The goal of the experiment is to probe the QCD phase diagram in the region of high baryon densities via measurements of multiplicities, phase-space distributions, and flow of protons, pions, kaons, hyperons, hadronic resonances, light vector mesons, charmonium, and open charm including their correlations and event-by-event fluctuations in heavy-ion collisions. For the performance of the system, its material budget is a crucial issue since multiple scattering in the detector materials will lead to a decrease in both track-finding efficiency and momentum resolution. There are different effects happening as a result of the interaction of particles with matter. The most important are the charged particles and here the main contribution, that can have a deteriorating effect on the performance, comes from ionization losses that are for heavy ions described by the Bethe – Bloch formula, secondary (delta) electrons production, and bremsstrahlung. In the case of ionization and delta electrons production, the losses and production rate are linearly proportional to the proton number. In the case of the bremsstrahlung, the effect has a quadratic dependence on the proton number. This is the main reason why carbon-based composite materials are preferred to iron-based ones.

An overview of the CBM experiment can be seen in Figure 1. A cave is currently under construction. Beams to HADES (High Acceptance Di-Electron Spectrometer) and CBM will be delivered by the SIS100 and SIS300 synchrotrons. The CBM experiment consists of a dipole magnet and several detectors: Micro Vertex Detector (MVD), Silicon Tracking System (STS), Ring Imaging Cherenkov detector (RICH), Muon Chambers (MuCh), Transition Radiation Detector (TRD), Time-of-Flight Detector (TOF), and Projectile Spectator Detector. In order to avoid scattering of the beam particles and very high speed collision products with air, a Beam Pipe with a vacuum inside is needed. The Beam Pipe has several main parts and starts directly after the target and goes through STS. This is the first main part. The second conical part connects to the STS and goes through RICH or MuCh, depending on the

configuration of the experiment. At the end of RICH or MuCh, a tilting mechanism is located. This mechanism is needed due to the different intensities of a magnetic field that will be used for different experiments. The last section is a straight one and continues through the TRD, TOF, and PSD and finally ends just in front of a beam dump, which is situated in the back wall of the cave. The experiment can be built in different configurations. There are rails on the ground on which the detectors can move, so there is no place to put static support for the last main part of the Beam Pipe. The modular solution is based on logistics and the cost of production requirements. [1] [2] [3] [4]

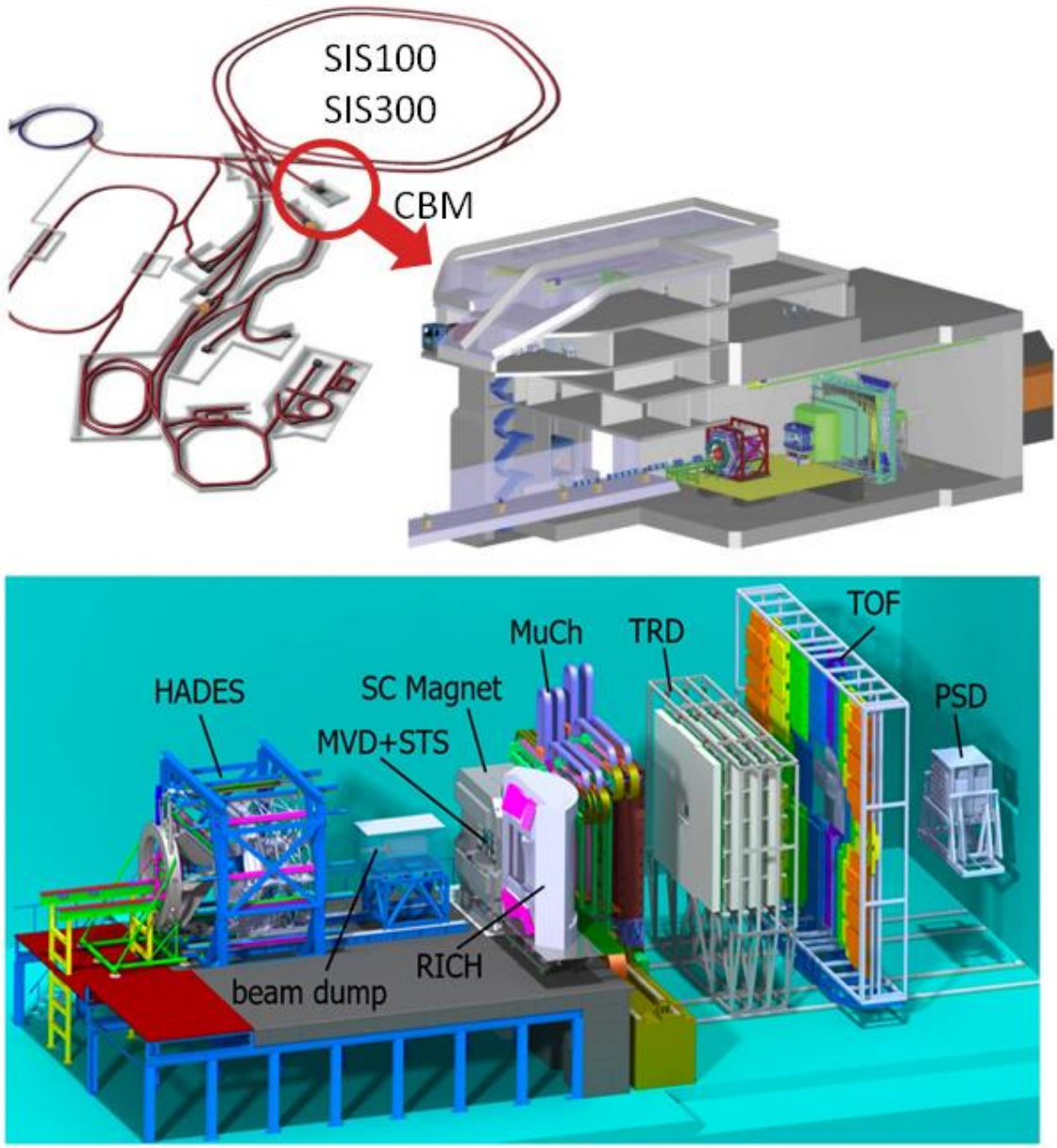

Figure 1: Overview of FAIR (up) and CBM Experiment (down) [4] [5]

2. Composite material

Composite materials, also called composition materials and shortened to composite, are nowadays used very often. We can find something made from a composite every day in our lives. The best example which everyone knows is reinforced concrete which is used in construction. Aircraft industries are using composites a lot due to their good strength to weight ratio and it is also the reason why is it used in motorsport, for example. Another reason why composite materials are appropriate for the Beam Pipe is their good radiation resistance.

Composites consist of two or more basic materials. These materials have different mechanical, chemical and physical properties. If these materials are combined together, a new material with different properties will be created. Parts made of composites can be even lighter, while retaining the same, if not greater, stiffness. Moreover, the composition of the composites can be determined precisely by the use of the part in industry.

On the other side, composites do not have only pros. Composite materials are pretty expensive and manufacturing parts made of composite is generally more expensive. Other disadvantage is that composites often need to be heat-treated by curing, which takes a lot of time. All pros and cons of material choice must be considered when designing.

In general, composites consist of two components: the matrix and the reinforcement. Reinforcements are there for distributing the stress to the construction and the matrix holds reinforcements together. The reinforcement can be imagined as a fibre (e.g. carbon fibre) and the matrix as a resin. Their structure can be made in several ways as shown in Figure 2.

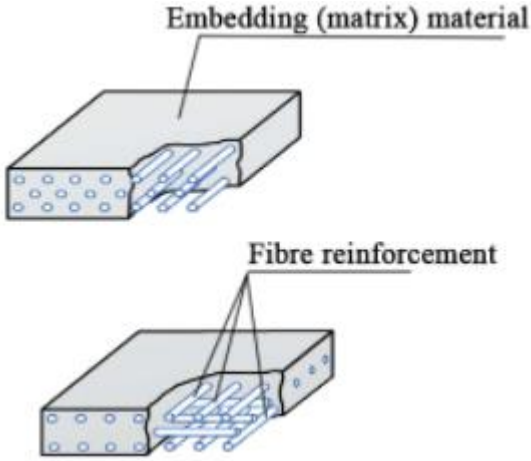

Figure 2: Structure of long fibre reinforced composite material in case of same oriented (up) and normal to each oriented (down) fibre reinforcement [6]

2.1. History of composite material

Composites began to appear first in the construction industry, when hay and mud began to be mixed to get better materials for building houses, later wood and dirt. Another historical use is Mongolian bows, which were made of bamboo kernels, silk, cattle tendons and horns and used pine resin as a matrix. After World War I, a composite known as bakelite

was invented, which was a mixture of cellulose and synthetic resin. Due to the needs of the army, the greatest expansion of composites came during and after World War II. Due to the good corrosion resistance, glass fibres have been widely used, especially in the shipbuilding industry. The biggest expansion in the commercial use of composites took place in the 1950s, mainly glass fibre. In the 1960s, Kevlar and carbon composite began to slowly emerge, primarily for the aerospace and space programs, automotive and shipping industries. [7]

2.2. Composite manufacturing techniques

The production of composite parts is very specific. For each piece, the manufacturing process needs to be selected correctly due to its function, material, performance, complexity, etc. After the composite piece is made, it can be further machined (for example, grooves for O-rings).

2.2.1. Open contact moulding

Open contact moulding is one of the oldest composite manufacturing techniques. This method is very simple. The fabric is placed in a mould and resin is then applied to it. The process is that first the form has to be treated with mould release, which is there to take the part out of the mould easily after the work is done. Then the mould is left to dry and laid with the first layer of resin. The fabric is carefully placed on the first layer of resin, so that it is correctly placed in all the hard-to-reach areas of the mould. The resin is then applied to the fabric again. The number of layers and their composition is completely arbitrary. Throughout the process, air is trapped between the layers and has to be removed by means of a roller or brush.

Creating can happen in several ways. The product can be cured at room temperature at atmospheric pressure - this is the simplest way. Alternatively, we can put a special separator sheet and breathable cotton on the last layer in the production. The whole mould is then put in a bag in which will create a vacuum. Alternatively, a piece can be cured at elevated temperatures and at atmospheric pressure. Autoclaves are used to achieve the best mechanical properties. These are large pressure chambers generating overpressure, into which we insert prepared products wrapped in a vacuum bag. External pressurization achieves even better air extraction from the product.

In this way, we can use all possible available fabrics. Kevlar, carbon or glass fibre fabrics are available. A pre-impregnated fabrics called Prepreg is also available. This is actually a basic fabric that is impregnated by the manufacturer and stored at low temperatures. When making few pieces, it is worth having Prepregs cut on a plotter for the mould. Once removed from the storage area (freezers), it is laid in a mould, vacuum-packed and then left to cure.

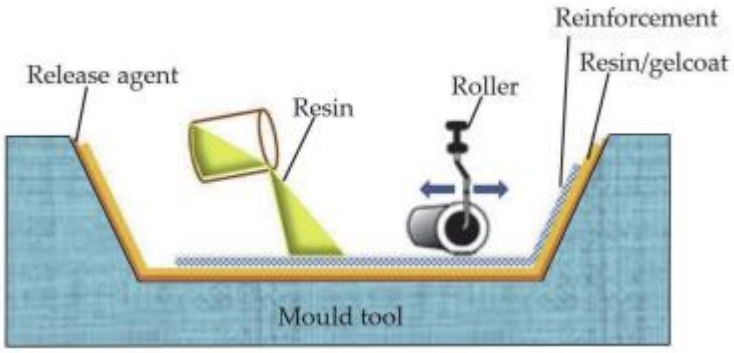

Figure 3: Hand lay-up process [8]

2.2.2. Resin infusion processes

This way of producing composite materials is based on the ever-increasing demand which necessitated faster production rates comparted to hand lay-up. It is also possible to use a greater degree of automation in this way.

The start is the same as hand lay-up, so the mould is first fitted with a mould release. Only dry fabrics are then placed in the mould. If the fabric is prepared directly for the form, it is only placed in the form, using the required number of layers and the desired composition. The layers are glued together with a special glue so that they don't shift towards each other. The mould is then closed and the low-viscous resins with the catalyst are pumped into the mould under pressure through the injection ports. [9]

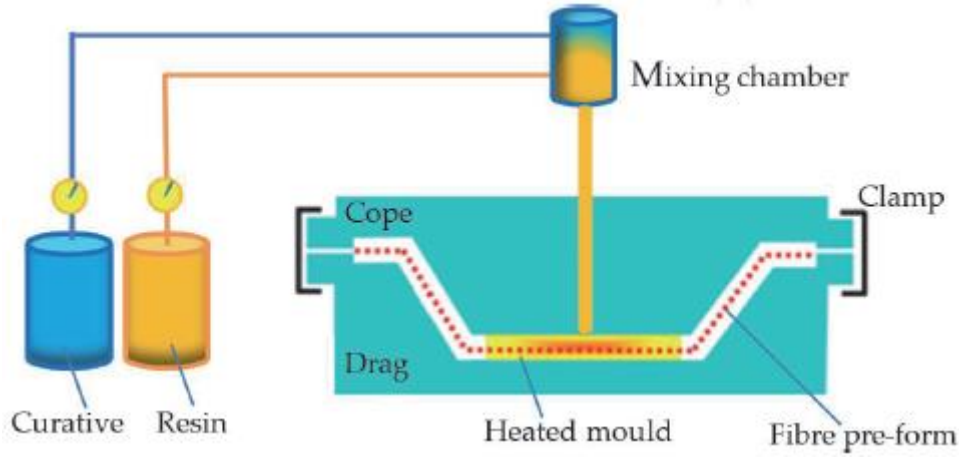

Figure 4: The schematic view of the resin infusion process [8]

2.2.3. Compression moulding

This method of making composite parts is very similar to hand lay-up. The process of putting the individual layers into the mould is exactly the same, except that it is no longer necessary to remove the air manually using rollers. The mould is made of two pieces that are in a hydraulic press and the upper part of the mould closes the lower mould with pressure after the layers are laid out. This situation is shown in Figure 5. In this figure an ejector pin is already shown, which is used for the easy removal of the final product. The charge is made from a soft material, which perfectly fits to lower mould under pressure.

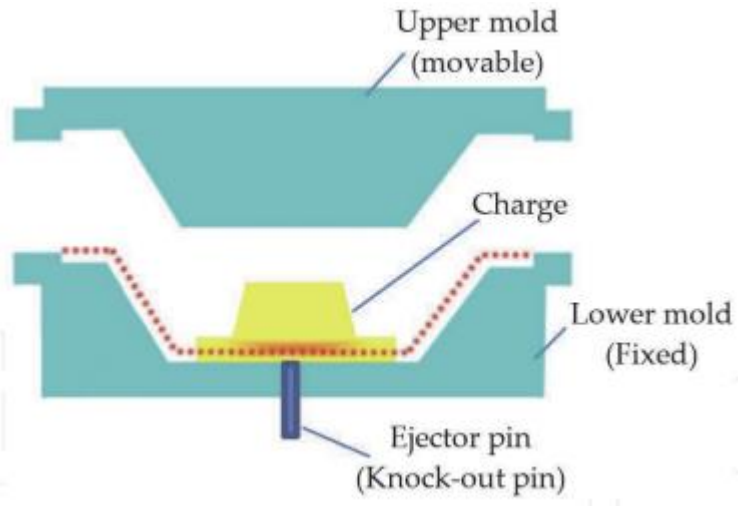

Figure 5: The schematic view of compression moulding process [8]

Alternatively, the form could be sealed with a flange, which will be fitted with an elastic surface and, by applying pressure, this surface becomes fixed and perfectly fits the mould. Air or compressed hot vapor can be used as a pressure source. Vapor would also speed up the curing process. Final products have good strength, they can be both complex and dimensional. This situation is shown in Figure 6.

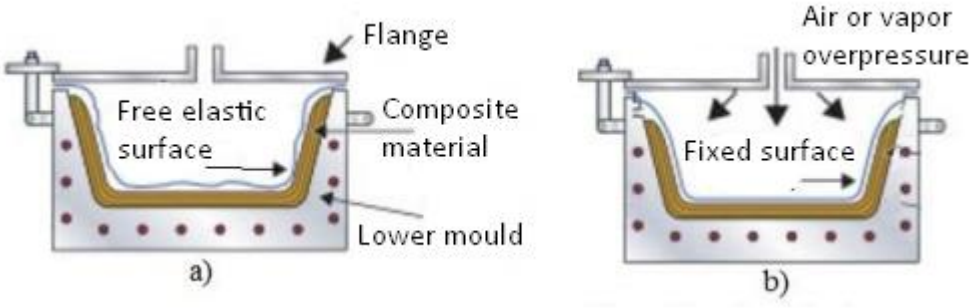

Figure 6: Alternative processes of compression moulding [10]

2.2.4. Pultrusion process

Pultrusion is a manufacturing process that was invented in the 1950s in the US. It allows the production of simple profiles, which are cut to the required length at the end of the process, e.g. tubes, screes, prisms. This method makes it possible to process fibres very quickly, and the resultant composite produced by pultrusion offers good quality, especially in comparison to hand lay-up composites, mainly due to curing at high temperatures.

The process begins by stretching the fibre itself, which is wound onto a roll. The fibre is drawn through a special grid that has the shape of the desired profile. Then the fibres are wetted with resin by drowning them in a resin bath. In the next step, the fibres continue to a heating chamber to be cured at high temperatures. After that, all that needs to be done is to cut the final profile to the required lengths. This process can be carried out continuously until the fabric runs out in the hopper.

In the past, the fibres were drawn in a resin bath, today epoxide is injected into them using pressure, which causes better saturation by resin. A significant advantage of this machine is its partial universality. It is not designed strictly for one type of composite, but composites from all types of fibres can be made on it using different types of resins. Furthermore, the profile shape depends only on the shape of the comparison grid. Currently, profiles can also be made curved. [11]

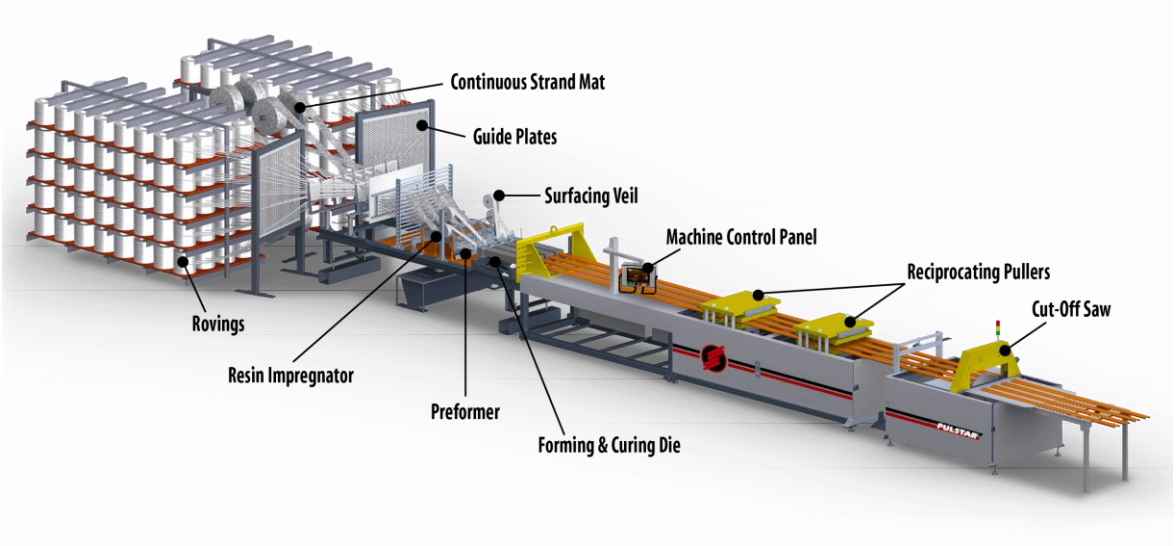

Figure 7: The schematic view of pultrusion process [11]

2.2.5. Filament winding

Presently, filament winding technology is one of the most efficient and progressive methods for producing hollow body composite materials. Glass, aramid or carbon fibre spools are used as reinforcements in the production process. These fibres are impregnated with a binding agent and then wound into a rotating mandrel that corresponds in shape to the product. The traverse carriage moves along an axis parallel to the mandrel, with the winding mandrel simultaneously rotating about its axis. The reinforcement is given a certain value of pre-stresses. The fibre warp angle can be regulated by the ratio of rotational speed to carriage speed, in the range from 0 ° to 90 °. All of these movements, and therefore the whole process of winding, are fully computerized, allowing optimization of kinematics exactly as required. This allows the precise laying of fibres in several axes, allowing for the production of components of relatively complex shapes. [12]

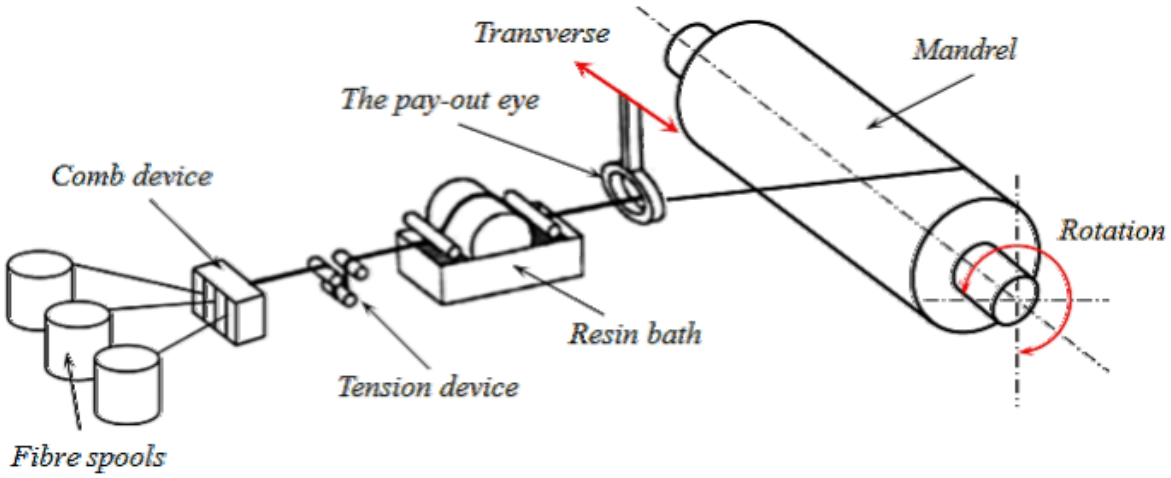

Figure 8: The schematic view of filament winding process [12]

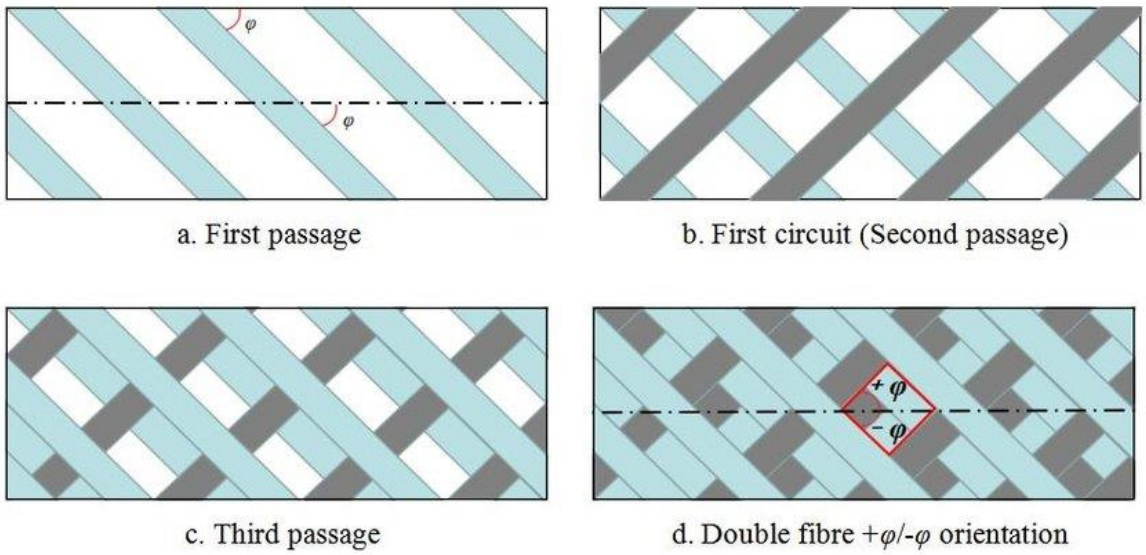

Figure 9: Filament winding process generation: (a) first passage, (b) first circuit, (c) third passage, (d) double fibre +φ/-φ fibre orientation [13]

3. Vacuum

One of requirement for the Beam Pipe is to contain vacuum. For the exact calculation of vacuum (pressure profile) sufficient knowledge is needed. Vacuum is an environment in which there is only a very small number of particles - ideally, no particles at all. In technical practice, a vacuum is characterised by a very low pressure relative to the surrounding environment.

3.1. Vacuum categories according to vacuum quality

Vacuum can be categorized into several categories as shown in Table 1. p is the absolute pressure in hPa, n is amount of molecules in a volume and λ is mean free path. Mean free path is the average distance travelled by a molecule between collisions with other molecules. [14] From Table 1 it is evident, that the required vacuum ($1 \times 10^{-3} hPa$) is in the medium to high range.

Table 1: Vacuum categories according to vacuum quality

Vacuum range	p [hPa]	n [$molecules/cm^3$]	λ [m]
Ambient pressure	1013	2.5×10^{19}	6.8×10^{-9}
Low vacuum	300 – 1	$10^{19} – 10^{16}$	$10^{-7} – 10^{-4}$
Medium vacuum	$1 – 10^{-3}$	$10^{16} – 10^{13}$	$10^{-4} – 10^{-2}$
High vacuum	$10^{-3} – 10^{-7}$	$10^{13} – 10^{9}$	$10^{-2} – 10^{3}$
Ultra-high vacuum	$10^{-7} – 10^{-12}$	$10^{9} – 10^{4}$	$10^{3} – 10^{8}$
Extremely high vacuum	$<10^{-12}$	$<10^{4}$	$>10^{8}$

A vacuum of different qualities is used in different industries and several examples are given as an overview: Vacuum is very often used in the food industry for vacuum packing and freeze drying. A low vacuum of 1 000 to 10 hPa is used. In the engineering industry, vacuum is very often used in casting. Namely in the production of super pure metals, where using vacuum we get undesirable elements out of liquid metals. In this field, vacuum values range from 300 to 10^{-11} hPa. Light bulbs are made using a vacuum of $1\text{-}10^{-4}$ hPa. Ultra high vacuum is used in particle accelerators, where the requirement is to have as few particles as possible in the accelerator itself. Here the vacuum reaches 10^{-6} - $10^{-14} hPa$. [15]

3.2. Vacuum pumps categories according to principle

Vacuum pumps are used to extract vacuum. Vacuum pumps are categorized according to the principle of their activity and the degree of vacuum achieved. Pumps can be broadly categorized according to three techniques [16]:

- Positive displacement pumps use a mechanism to repeatedly expand a cavity, allowing gases to flow in from the chamber, seal off the cavity, and exhaust it to the atmosphere.

- Momentum transfer pumps, also called molecular pumps, use high speed jets of dense fluid or high speed rotating blades to knock gaseous molecules out of the chamber.
- Entrapment pumps capture gases in a solid or absorbed state. This includes cryopumps, getters, and ion pumps.

3.3. Vacuum pumps categories according to vacuum quality

Each type of vacuum pump can achieve a different quality of vacuum, so they are also categorized by this criterion as follows [17]:

- Pumps for ambient pressure (up to 300 hPa)
  - Diahpragm pump
  - Liquid ring pump
- Pumps for low vacuum (300 – 1 hPa)
  - Rotary plunger pump
  - Piston pump
  - Scroll pump
  - Screw pump
- Pumps for Medium vacuum (up to 10^{-3} hPa):
  - Rotary piston pump
  - Rotary vane pump
- Pumps for High vacuum (up to 10^{-7} hPa):
  - Diffusion ejector pump
  - Vapor jet pump
  - Adsorption pump
  - Roots pump
- Pumps for ultra-high vacuum (up to 10^{-12} hPa):
  - Ion sputter pump
  - Turbomolecular pump
  - Diffusion pump

Depending on the categorisation above, several different types of vacuum pumps may be chosen for the specified vacuum 10^{-3} hPa. At first glance, a combination of a rotary and diffusion pump, for example, would be an appropriate choice. However, the diffusion pump could be used on the primary stage. There, the great advantage is the possibility of constructing it to large dimensions and therefore high pumping speed. However, both the rotary vane pump and the diffuse vacuum pump work with oil and this is their biggest disadvantage. Moreover, diffusion has a large energy consumption.

The fact that the diffusion and rotation pumps are working with oil is a problem for particle accelerators. In particle accelerators, there is a requirement for the cleanest

possible environment. Today's trend is to use scroll pump and turbomolecular pump combinations, which is why these two types of pumps will be addressed in more detail.

3.4. Scroll pump

The scroll vacuum pump is as a dry vacuum pump because it does not use any working fluid and therefore does not suffer from problems with the diffusion of the working fluid vapour back into the pumped chamber. The scroll pump consists of a stator and an eccentrically moving spiral-shaped rotor, as shown in Figure 10. The surfaces through which the spirals touch each other are fitted with PTFE for tightness. The vacuum pump inlet is at the edge of the vacuum pump and the gas is compressed towards the centre of the vacuum pump where the vacuum pump outlet is located.

This type of vacuum pump can have atmospheric pressure at the outlet. It can be used separately for vacuum up to $10^{-2}\ hPa$, or as a forepump. As a forepump it will be used in combination with a vacuum pump that cannot have atmospheric pressure on the inlet. As mentioned above, it is most commonly used in combination with a turbomolecular vacuum pump. [18]

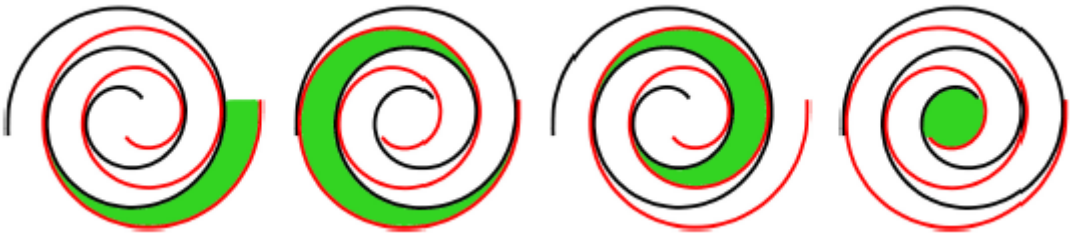

Figure 10: Construction and functional principle of scroll vacuum pump [18]

The performance characteristics of this type of vacuum pump depend on several factors, including the unit size, speed of operation, ambient temperature and characteristics of the gas or vapour being pumped. In general, the ultimate pressure is approximately $10^{-2}\ hPa$, pumping speed is between 3 and 60 m^3/hr, leak tightness is less than $10^{-6}\ l/s$, noise is less than 55.4 $db(A)$ and suck-back protection is provided by an exhaust valve. [19]

3.5. Turbomolecular pump

For the same reasons as a scroll vacuum pump, a turbomolecular pump is included among dry pumps. In terms of construction, it consists of a rotor and a stator consisting of several rows of blades tilted at different angles. The gas molecules collide with the blades of the rotor and stator, giving them an additional component of speed towards the output. Turbomolecular vacuum pumps can only be used in combination with a forepump that produces a pressure of approximately $10^{-1}\ hPa$. The rotor of this vacuum pump reaches a very high revolutions speed which is from 24 000 to 90 000 $1/min$. Their typical operating range is between $10^{-3}\ hPa$ and $10^{-11}\ hPa$ and pumping speed is between 10 and 4 000 l/s.

Two basic turbomolecular vacuum pump designs are available, namely a horizontal arrangement and a vertical arrangement, both shown in Figure 11. [18]

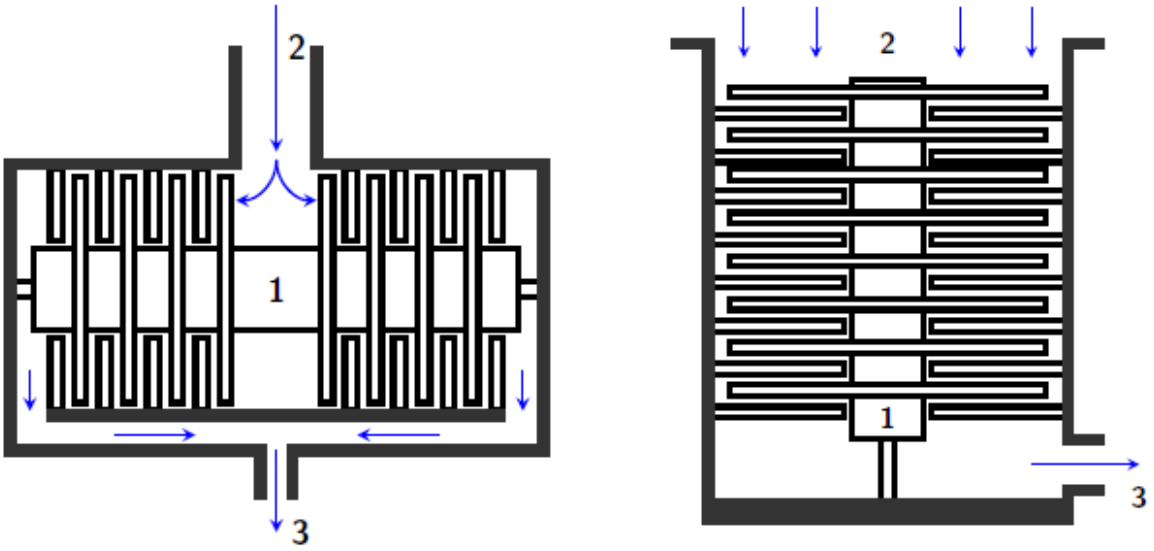

Figure 11: Construction types of turbomolecular vacuum pumps – horizontal arrangement in the left and vertical arrangement in the right. 1 – rotor, 2 – inlet, 3 – outlet [18]

An interest in turbomolecular vacuum pumps is the rotor housing. When invented in 1954, the rotor on both ends was held in mechanical bearings. However, these require lubricant and the lifetime of the pump is determined by the bearings lifetime. In addition, mechanical bearings cause the pump's dynamic properties to be less favourable. On the other side, they are resistant to external shocks and possessing a small footprint.

An alternative to mechanical bearings are the five-axis active magnetic bearings. This type of bearing does not require any lubrication, the life of the pump is not limited by the bearing life and there is very low vibration transmission. Due to absence of mechanical bearings, turbomolecular vacuum pumps are also suitable of pumping corrosive gases that would destroy the lubricated mechanical bearings in short period of time. On the other hand, these bearings are less shock-resistant, more expensive and have larger footprint. Turbomolecular pumps with active magnetic bearings are manufactured either with magnetic bearings at both ends of the rotor shaft, or with mechanical bearing in the lower end of the shaft (for vertical arrangement) and with active magnetic bearing in the upper end of the shaft. Combination mechanical and magnetic bearings are called hybrid bearing and a fully levitated turbomolecular vacuum pump uses only magnetic bearings. [20]

3.6. Vacuum Connections

3.6.1. Non-detachable connections

Non-detachable connections in vacuum technology are achieved by welding, brazing or fusing, or by metalizing or sintering with subsequent brazing. In recent years, vacuum-resistant adhesives have also come into use to join components for applications that do not involve UHV technology. The chosen connection technology must be appropriately designed for the major requirements with respect to mechanical strength,

temperature and alternating thermal loads, as well as the required gas-tightness. Material pairings such as metal-to-metal, glass-to-glass, glass-to-metal, metal-to-ceramic and glass-to-ceramic are used relatively frequently in vacuum technology. Metals are most often joined by means of welding and brazing. In glass equipment, the individual glass components are joined through fusion. Metal and glass connection by fusing or metalizing and fusing or brazing are used for UHV-compatible, bakeable viewports. Metals and ceramic connections produced by metalizing or sintering are common, for example, for vacuum current feedthroughs. [15]

3.6.2. Detachable connections

The individual components of a vacuum system, e.g. vacuum chambers, pumps, valves, measurement instruments, etc., are connected with one another either directly or by means of pipe components or resilient elements. The detachable interfaces between the components must be vacuum-tight. In configuring a vacuum system, however, as few detachable joints as possible should be used, as they represent a significantly more frequent source of potential leakage than non-detachable joints. Flange components from stainless steel, aluminium and steel can be used as connection elements. Metal hoses made of stainless steel are preferable to thick-walled rubber or thermoplastics for flexible joints. They are a strict necessity from the lower medium vacuum range onward. [15]

From low to high vacuum ranges, ISO-KF flange connections with nominal widths of DN 10 to DN 50 are used for detachable connections, for larger nominal sizes of DN 63 to DN 1000 ISO-K and ISO-F flanges are used. Ultra-high vacuum compatible releasable connection, are in nominal widths DN 16 to DN 400 as a CF flange connection, respectively for larger nominal diameters of DN 400 to DN 800 flanges as a COF flange. [15]

3.6.2.1. ISO-KF flange

An ISO-KF connection consists of two symmetrical flanges and one O-ring seal, which is positioned and supported with an internal or external centering ring. The necessary pressing force for the sealing is created by a clamping ring, which is placed over the conical tightening area and is tightened with a wing screw. This allows for a fast, efficient assembly and disassembly without any tools. The flanges can be aligned around its main axis in any direction. These connections are suitable for pressures up to 10^{-8} hPa and with metal seals, the pressure range can be extended to less than 10^{-9} hPa. They are described in DIN 28403 and ISO 2861 in nominal diameters DN 10 to DN 50. [15]

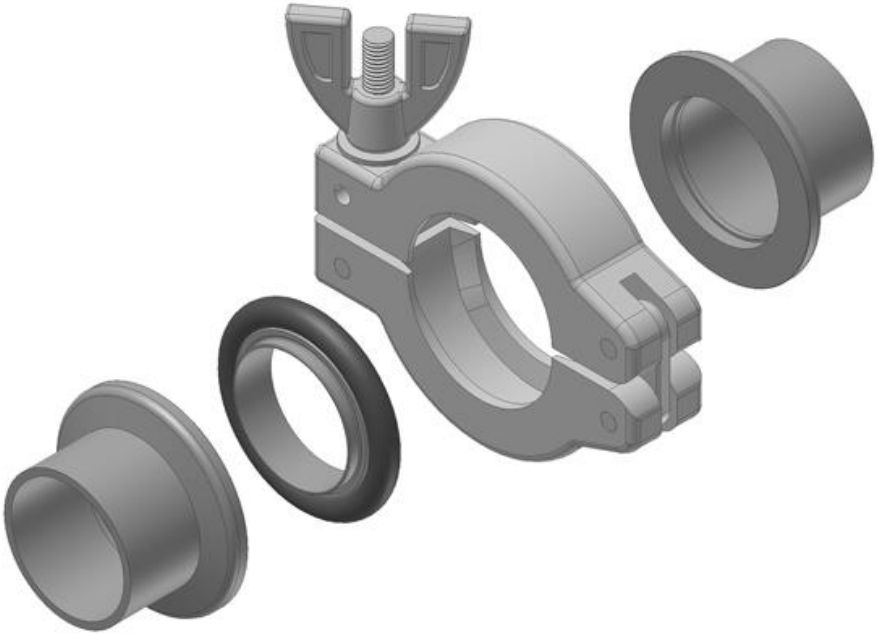

Figure 12: ISO-KF flange assembly [21]

3.6.2.2. ISO-K flange

Two single flanges are connected with the help of claw clamps. The flanges have a groove on the back in which the claw clamps are hooked which press the flanges together. As with KF connections there is a sealing with centering ring and O-ring between the flanges. Mostly an additional trapped centering ring is used which produces an assembly with constant distance. [21] This type of connection is suitable for pressures up to $10^{-8}\ hPa$ and with metal seals the pressure range can be extended to less than $10^{-9}\ hPa$. They are described in DIN 28404 and ISO 1609 in nominal diameters from DN 10 to DN 630.

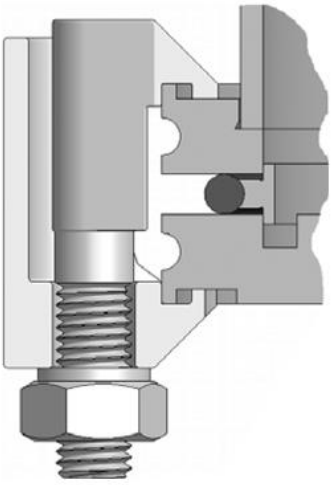

Figure 13: ISO-K flange [21]

3.6.2.3. ISO-F flange

ISO-F flanges are essentially ISO-K flanges with holes. The sealing principle is the same as for ISO-K flanges. Both flanges can be combined with each other easily. Flanges are held

together using bolts. This type of connection is suitable for pressures up to 10^{-8} hPa and with metal seals the pressure range can be extended to less than 10^{-9} hPa. They are described in DIN 28404 and ISO 1609 in nominal diameters from DN 10 to DN 630. [15]

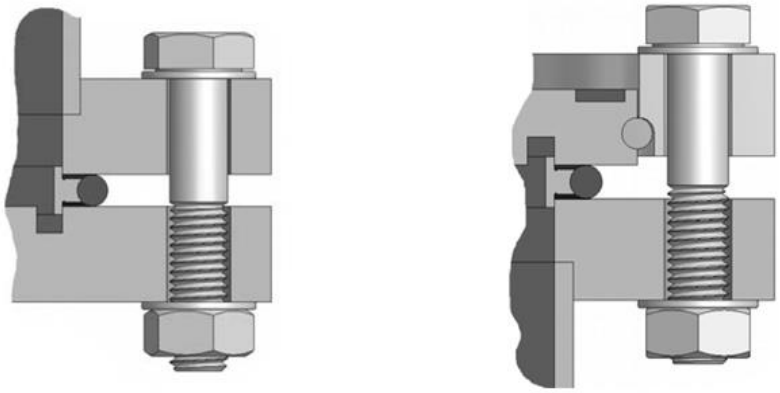

Figure 14: ISO-F flange

3.6.2.4. ISO-CF flange

These flanges are commonly used for ultra-high vacuum, which poses great demands on the material and connections. They are manufactured from circular blanks of stainless steel on CNC machines. Rotatable flanges are bipartite and consist of an inner part with the seal face and an outer part with the bolt holes. CF flanges have an annular groove on the vacuum side for the reception of the gasket and a knife-edge. Sealing is achieved by means of a flat gasket of oxygen-free copper because of the low leak rate and high bakeout temperature necessary for UHV technology. This gasket can be used generally only once due to the plastic deformation by the knife-edge. [21] They are described in ISO 3669 in nominal diameters DN 16 to DN 250 and detailed in ISO/TS 3669-2 in nominal diameters DN 10 to DN 400. This connection type is suitable for pressure less than 10^{-12} hPa. It can be used sealing made of FKM several times, but only for pressures less than 10^{-8} hPa. [15]

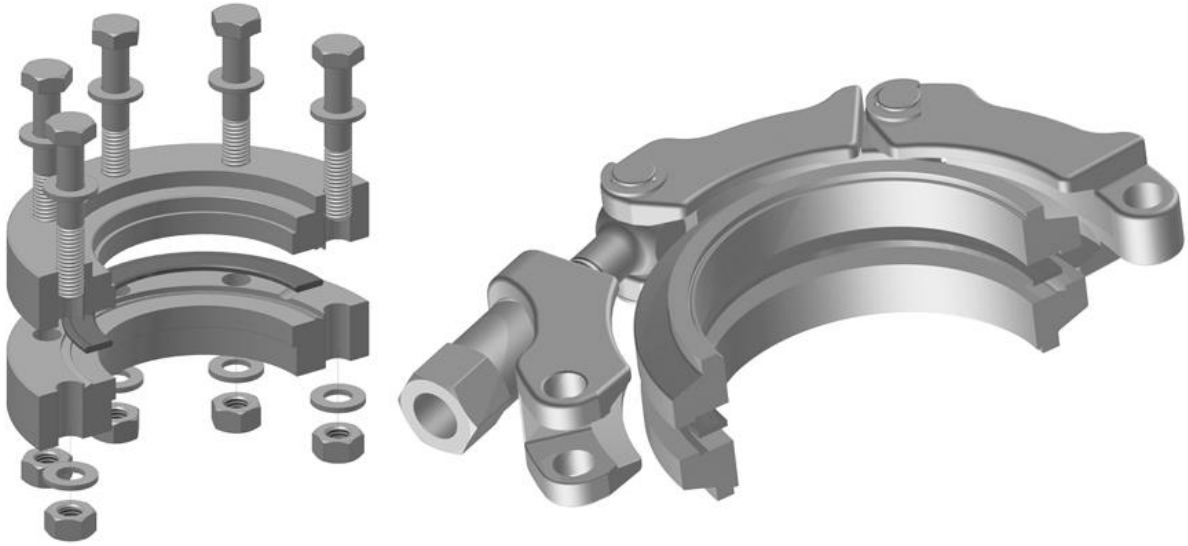

Figure 15: ISO-CF flange [21]

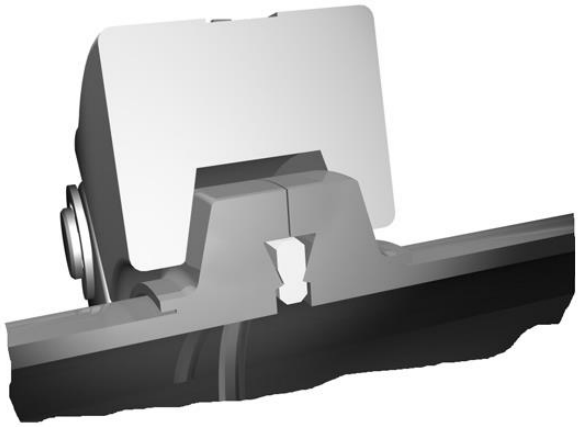

Figure 16: Detail of sealing of ISO-CF connection [21]

3.7. Vacuum conductance

Conductance is defined as a ratio of throughput to pressure differential, under steady conditions, where the pressures refer to two isobaric sections inside the pumping system, as shown in Figure 17 [22]. With the basic equation of vacuum technology:

$$P = \frac{Q}{S} \tag{1}$$

Where P is pressure in $[Pa]$, Q is gas load in $\left[Pa \cdot \frac{m^3}{s}\right]$ and S is pumping speed in $[m^3/s]$

It is one of the primary concepts through which many other quantities can be calculated, such as the effective pumping speed and the average pressure.

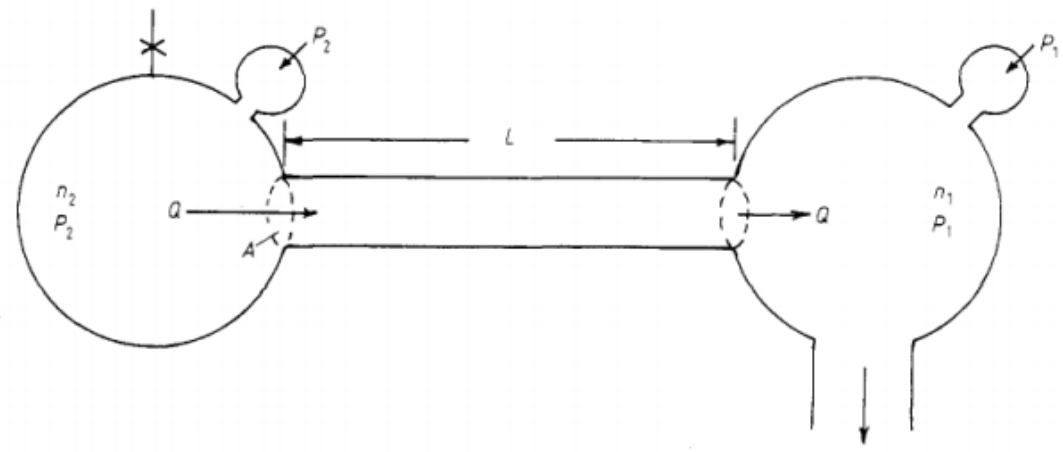

Figure 17: The schematic view of vacuum conductance

3.8. Pressure profile

For the design of vacuum inputs, it is necessary to know where those vacuum inputs will be located. Due to the limited (i.e., not infinite) conductance of the tube, pressure will have maximums at equal distance from two vacuum pumps and minimums above the

vacuum pumps. Figure 18 shows that the pressure in long tubes is dependent on the distance to the vacuum pump.

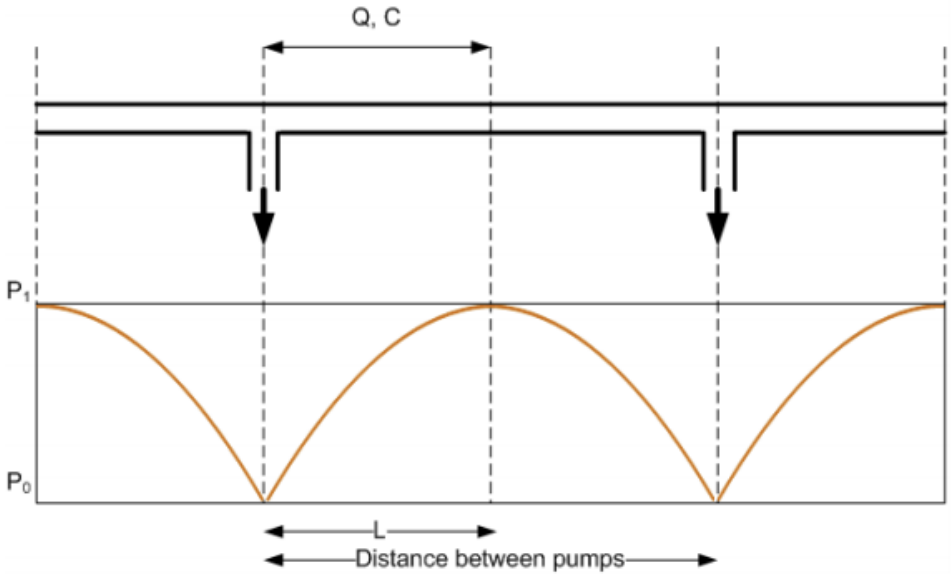

Figure 18: Pressure profile (red) in long tube

3.9. Gas release from solids

When we create vacuum, we're actually not just removing the gas that's inside the container, but the gases that are appearing there in addition. The gas is dissolved and adsorbed on solids. This gas release, commonly referred to as outgassing, is the result of several different processes as shown in Figure 19. The gases and vapours emitted on the surface are a consequence of a vaporization, diffusion, permeation, thermal desorption and stimulated desorption [23].

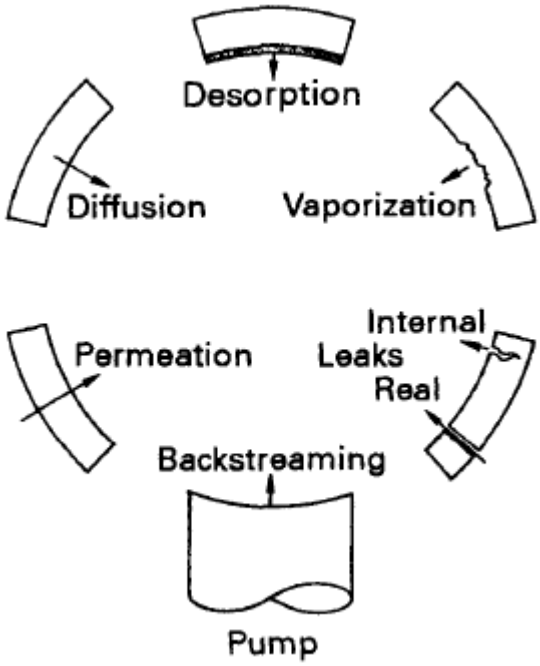

Figure 19: Potential sources of gases in vacuum systems [23]

- *Vaporization* is the thermally stimulated entry of molecules into the vapor phase, as steam is a gas above its condensation temperature. On the inner surface of the Beam Pipe, this causes the material to evaporate. [23]
- *Diffusion* is the transfer of molecules of one material through another. Gas diffusion to the interior wall of a vacuum system followed by desorption into the chamber contributes to the system outgassing. The gas pressure in the solid establishes a concentration gradient that drives molecules or atoms to the surface, where they desorb. Because diffusion is often a much slower process than desorption, the rate of transport through the bulk to the surface will usually govern the rate of release into the vacuum. [23]
- *Permeation* is a three step process. First, the gas is adsorbed on the outside wall of the vacuum chamber, then passes through its bulk and finally desorbs from the inside wall. Permeation through glass, ceramics and polymeric materials is molecular. [23]
- *Thermal desorption* is the heat-stimulated release of gases or vapors previously adsorbed on the interior walls of the system. The vapours could have been adsorbed on the surface of the container while it was exposed to gas extraction. [23]
- *Stimulated desorption* is caused by the impact of electrons, atoms, molecules, ions or photons on a solid surface, allowing them to release adsorbed gases and create vapors in quantities that are enough for setting limit of the final pressure in the vacuum chamber. [23]

- *Leaks* are undesirable occurrences, caused for example by a damaged O-ring, and must be avoided.
- *Backstreaming* occurs in a vacuum pump by moving the molecules back into the vessel.

3.10. Numerical method for calculating pressure profile

Numerical calculation methods are very useful for accurate calculation, especially for ultrahigh vacuum. Because particles in a vacuum move randomly, it is necessary to simulate their movement. The particles bounce off the walls at a random angle, similarly hitting another particle. Most likely, the particles will bounce in a direction perpendicular to the surface, and the probability of the direction of the reflection is given by the Knudsen Law (cosine probability distribution). [18]

In 1990, the first version of the Molflow+ program was written by Robert Kersevan. The program can simulate particle flights, particles wall reflections, their collisions, and more. It uses the Monte Carlo simulation to simulate particle routes.

The input to the program is the geometry in which the particles move, which can be created in any CAD program. After importing geometry, it is need to set simulation parameters. Here it can be set where the particles are coming from in the vacuum chamber (outgassing, desorption) as well as the position of the pumps. In the end, the desired output has to be specified. Figure 20 shows how particle trajectories can look like and in the same figure particles escaping from the system are visualised.

The measured output can be the pressure anywhere on the surface of the imported geometry, or also in the centre of the volume as shown in the Figure 21. It also shows that the quality of the vacuum is changing and the number of particles is increasing with the distance from the vacuum pump, which is located on the left side. [24]

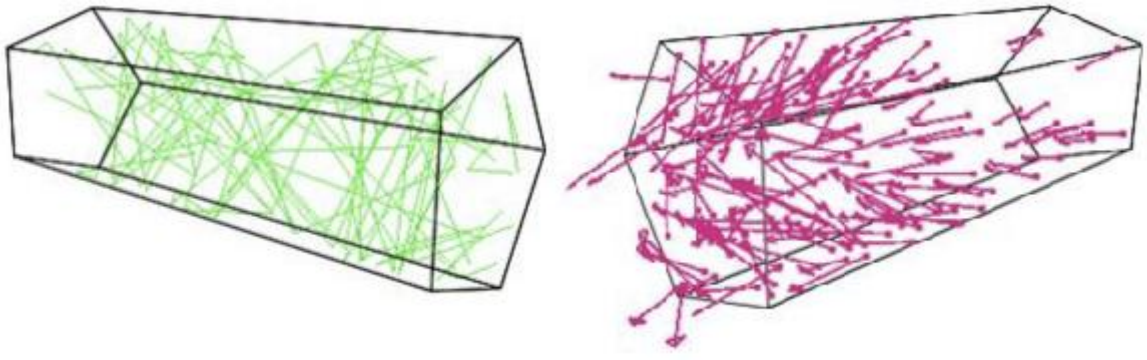

Figure 20: Particle trajectories in the left and visualized particles escaping from the system in the right [24]

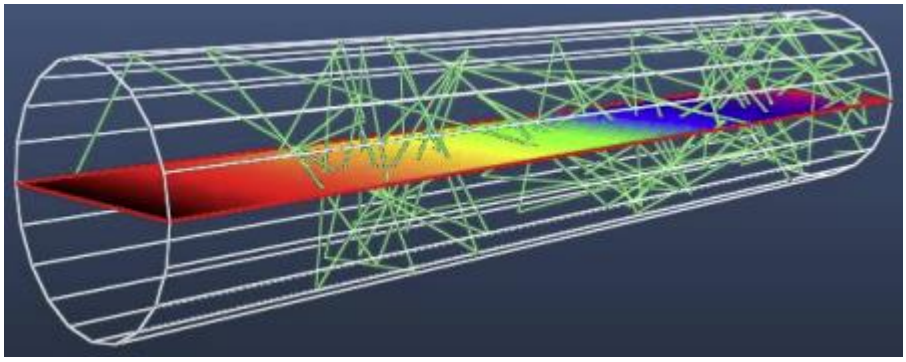

Figure 21: MolFlow+ simulation result [24]

3.11. Vacuum calculation

The specification implies that it is necessary to design the number and positioning of vacuum inputs so that the vacuum is $10^{-3}\ hPa$ or less. For the initial design, the procedure is to chose a suitable type of turbomolecular vacuum pump from a catalog . A vacuum pump with a pumping speed of 33 l/s has been selected. [15] This pump speed is only achieved if the vacuum pump is located directly on the Beam Pipe. This is most likely not to be this case, therefore the pumping speed will be lower and a pump will have to be selected after accurately determining the location of the vacuum pump and the piping to it. In the available literature, which relates to pressure profile calculations, the problem of vacuum quality and the associated number of inputs and their positioning is discussed for vacuum of quality $10^{-7}\ hPa$ and more. Based on this, it was decided to check the pressure difference at both ends of the pipe.

The type of flow in the Beam Pipe has to be decided first. This will be achieved by calculating the Knudsen number, whis is calculated as follows:

$$Kn = \frac{\lambda}{D}\ [-] \tag{2}$$

Where λ is mean free path and D is inner diameter of the Beam Pipe. $D = 176[mm]$ and λ is pressure dependent and has value $\lambda = 10^{-1}\ [m]$ for pressure $10^{-3}\ mbar$. Then can be calculated:

$$Kn = \frac{\lambda}{D} = \frac{1}{176 \cdot 10^{-3}} = 0.568\ [-] \tag{3}$$

For $Kn < 0.01$ is continuous flow; for $0.01 < Kn < 0.5$ is Knudsen flow and for $Kn > 0.5$ is molecular flow. It is obvious that for $Kn = 0.568$ it is a molecular flow.

In the next step, it is need to calculate the conductance. In the literature it is possible to find a lot of different formulas for conductance calculation. For this case, it is needed to take the formula for molecular flow and a long circular tube. The conductance of a long round tube is calculated as shown: [14]

$$C_L = 12.4 \cdot \frac{D^3}{L}[l/s], where\ D, L\ in\ cm \tag{4}$$

And for this case:

$$C_L = 12.4 \cdot \frac{D^3}{L} = 12.4 \cdot \frac{17.6^3}{1462} = 46.24[l/s] \tag{5}$$

Now it is need to calculate the outgassing rate on the surface. So it is needed to calculate the surface of the pipe and multiply it by the outgassing rate, which for this case is $q = 1.333 \cdot 10^{-7}\left[\frac{hPa \cdot l}{s \cdot cm^2}\right]$. [25]

$$S = \pi \cdot D \cdot L = \pi \cdot 17.6 \cdot 1\,462 = 80\,836\ [cm^2] \tag{6}$$

$$Q = q \cdot S = 1.333 \cdot 10^{-7} \cdot 80\,836 = 1.078 \cdot 10^{-2}\left[\frac{hPa \cdot l}{s}\right] \tag{7}$$

For the calculation of maximum and minimum pressure, the formulas below are used [14]:

$$p_{min} = \frac{2Q}{S}[hPa] \tag{8}$$

$$p_{max} = p_{min} + \frac{Q}{2C_L}[hPa] \tag{9}$$

Where S is the effective pumping speed including a correction for the connecting element. Assuming $S = 33\ [l/s]$, the final results will be:

$$p_{min} = \frac{2Q}{S} = \frac{2 \cdot 1.078 \cdot 10^{-2}}{33} = 6.531 \cdot 10^{-4}\ [hPa] \tag{10}$$

$$p_{max} = p_{min} + \frac{Q}{2C_L} = 1.437 \cdot 10^{-4} + \frac{1.078 \cdot 10^{-3}}{2 \cdot 46.24} = 7.696 \cdot 10^{-4}\ [hPa] \tag{11}$$

The result shows that at the end of the Beam Pipe, the pressure will still be less than the required value. Unfortunately, we cannot apply the same procedure to multiple points and multiple lengths, respectively, in order to determine the pressure profile depending on the distance from the vacuum inlet. For this purpose, a formula from [26] is used.

$$P(x) = p_{min} + \frac{\pi \cdot q}{2 \cdot k \cdot D^2} \cdot (2 \cdot x \cdot L - x^2) \tag{12}$$

Where

$$k = C_L \cdot \frac{L}{D^3} \tag{13}$$

It is evident that:

$$k = 12.4 \cdot \frac{D^3}{L} \cdot \frac{L}{D^3} = 12.4 \left[\frac{hPa \cdot l}{s \cdot cm}\right] \tag{14}$$

This gives us an equation that shows the pressure profile. The equation has been processed using MS excel and the resultant plot shown in Figure 22 shows the result. From the plot, there can be seen that the pressure is gradually rising and converts to a calculated p_{max}.

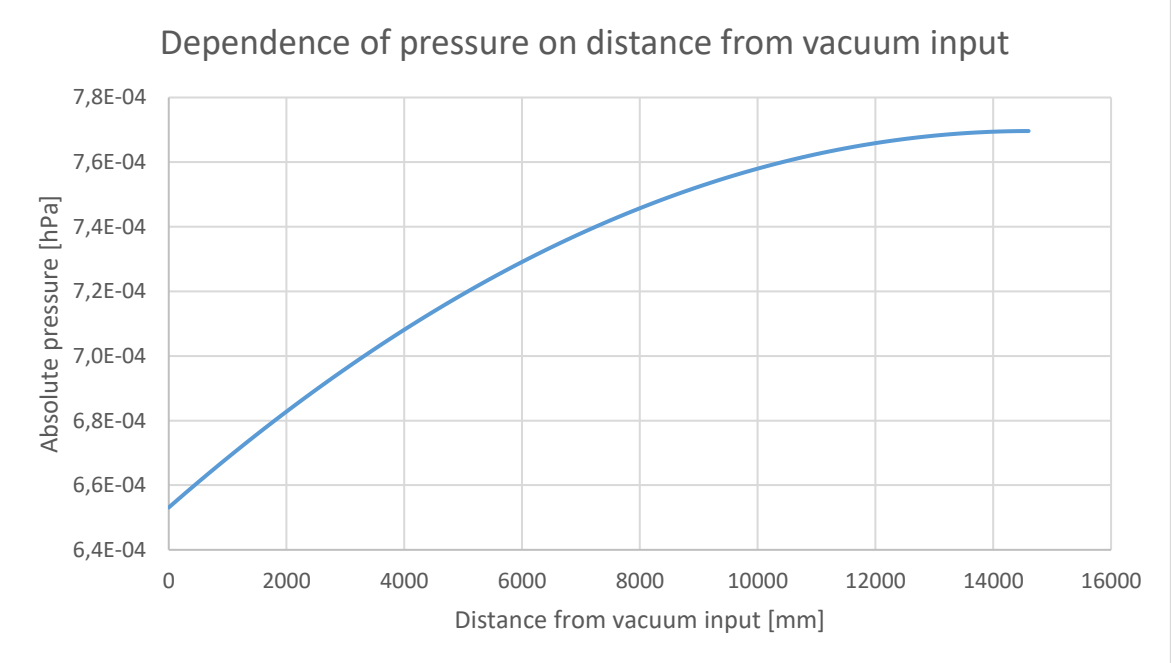

Figure 22: Dependence of pressure on distance from vacuum input

4. O-rings

O-rings are circular sealing elements with high precision. In design, they offer a very efficient, reliable and economically advantageous sealing element for a wide range of static or dynamic applications. The rings are manufacturing by vulcanising in moulds and can also be used as double sealing. Ring size is defined by inner diameter d_1 and ring thickness d_2, as shown in Figure 23.

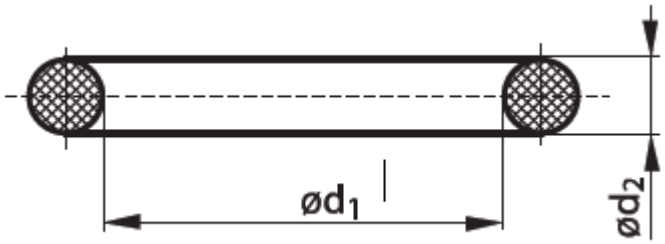

Figure 23: Section cut through O-ring [27]

The following table shown in Figure 24 gives an overview of material groups of elastomeric substances with the option of choosing the material hardness. For our purposes FPM material was chosen, also called Viton due to its good properties for vacuum sealing. The most important factors for designing the right O-ring hardness are the value of operating pressure and the width of the sealing joint. The diagram shown in Figure 25 is showing the dependence between pressure (x axis) and seal joint width (y axis) in static applications. From the graph it is evident that choosing the hardness of the O-ring for our purpose is not so important. There is need to only seal a pressure of 1 hPa which is caused by vacuum.

Code	Trade name	Hardness Shore A
NB, NBR	Nitrile-butadiene-rubber	55, 60, **70**, 75, **80**, **90**
FP, FPM	Fluorine rubber (Viton)	60, 70, 75, **80**, 90
SI	Silicone rubber	50, 60, **70**, 80
EP, EPDM	Ethylene-propylene rubber	75, 80, 85
CR	Chloroprene rubber	50, 60, 70, 90
NR	Natural rubber	45, 65, 80
BU	Butyl rubber	45, 65, 80
CSM	Chlorsulphonated polyethylene rubber (Hypalon)	65, 75
PTFE	Polytetrafluoroethylene (Teflon)	-

Figure 24: Material of O-rings [27]

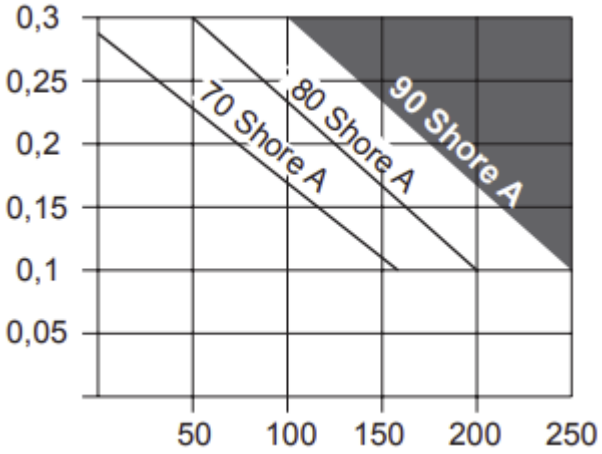

Figure 25: Dependence between O-ring hardness and pressure [28]2

4.1. Dimensions of groove for O-rings

It is always advisable to choose O-rings with the largest thickness d_2 possible as they have several advantages compared to O-rings with lower d_2 values. There are three main advantages which are: lower abrasion which means higher service life, lower deformation and larger contact surface. But for this case where the material budget needs to be as low as possible, one of the smallest thicknesses available for a specified value (184 mm) was chosen. Dimensions of the grooves for O-rings used for vacuum sealing are different than sealing used for overpressure. For vacuum sealing it is needed that the O-ring fills the groove as tightly as possible so that no leakage occurs as a result of shrinkage of the elastomeric substance in the vacuum. It is necessary to prevent the O-ring from moving in the groove. The processing of sealing surfaces should be carried out with the greatest possible care. In Table 2Table 1 groove dimensions for vacuum sealing are shown.

Table 2: Dimensions of groove for O-rings for vacuum [27]

Thickness d_2 [mm]	1.80	2.65	3.55	5.30	7.00
Depth t [mm]	1.30	1.95	2.60	3.90	5.15
Width b [mm]	2.20	3.10	4.10	6.10	7.85

Since the O-rings are processed by vulcanizing the elastomer, dimensional changes occur due to shrinkage. Tolerances for the inside diameter d_1 are shown in Table 3. Since the tolerance is relatively big and O-rings are pliable enough, it is not necessary to have exactly the same dimension that we need.

Table 3: Dependce of diameter d_1 tolerances to its main dimension [28]

Inner diameter d_1 [mm]	Tolerance d_1 ± [mm]
$170 < d_1 \leq 175$	1.38
$175 < d_1 \leq 180$	1.41
$180 < d_1 \leq 185$	1.44
$185 < d_1 \leq 190$	1.48
$190 < d_1 \leq 195$	1.51

Dimensions of grooves for several O-rings thickness are shown in Table 2. The O-ring chosen from the catalogue has a thickness, that is not listed in the Table 2. For this reason,

the dimension for the O-ring which will likely be used, needs to be calculated. It will be calculated for thicknesses of 1.5, 2, 2.5 and 3 mm. The calculation will use a mathematical similarity and will use dimensions of d_2 = 3.55 mm; t = 2.60 mm; b = 4.10 mm

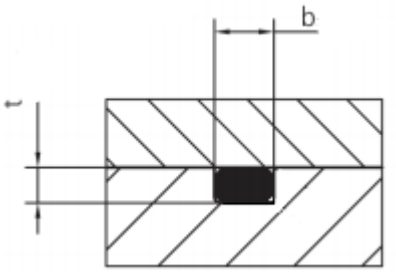

Figure 26: Dimensions of groove for O-ring

First of all, the area of the groove needs to be known as well as the area of the O-ring cross section:

$$A_{groove} = b \cdot t = 4.1 \cdot 2.6 = 10.660\ [mm^2] \tag{15}$$

$$A_{section} = \frac{\pi \cdot d^2}{4} = \frac{\pi \cdot 3{,}55^2}{4} = 9.898\ [mm^2] \tag{16}$$

Now it is evident that the groove is big enough for the O-ring. The ratio between these numbers will be used to calculate the area of the new size of the O-ring:

$$A_{ratio} = \frac{A_{groove}}{A_{section}} = 1.077\ [-] \tag{17}$$

In the next step, the area of the section for the new size will be calculated, which will be 2 mm:

$$A_{section_2} = \frac{\pi \cdot d^2}{4} = \frac{\pi \cdot 2^2}{4} = 3{,}141\ [mm^2] \tag{18}$$

$$A_{groove_2} = A_{ratio} \cdot A_{section_2} = 1.077 \cdot 3.141 = 3.383\ [mm^2] \tag{19}$$

With the areas known, just the depth and width have to be calculated to get the final dimensions of the groove for the O-ring. Similarity will again be used, and from the ratio between the depth and the width the dimensions will be calculated for the new size:

$$ratio = \frac{b}{t} = \frac{4.1}{2.6} = 1.769 \tag{20}$$

$$A_{groove_2} = ratio \cdot t_2^2 \rightarrow t_2 = \sqrt{\frac{A_{groove_2}}{ratio}} = \sqrt{\frac{3.383}{1.769}} = 1.383\ [mm] \quad (21)$$

$$b_2 = t_2 \cdot ratio = 2.447\ [mm] \quad (22)$$

If the results are to be altered, the final dimensions of the groove for O-ring will be: $b \times t = 2.45 \times 1.4\ mm$. To check, this area will be calculated and compared to the O-ring area size:

$$A_{groove_{new}} = 2.5 \cdot 1.4 = 3.5\ [mm^2] \quad (23)$$

$$A_{groove_{new}} > A_{groove_2}$$

By the same method, more dimensions were calculated, and the results are listed in the following table:

Table 4: Results of groove for O-ring dimensions dependent do d_2

Thickness d_2 [mm]	1.5	2	2.5	3
Depth t [mm]	1.1	1.45	1.8	2.2
Width b [mm]	1.7	2.3	2.9	3.45

5. Design

Several problems had to be solved when designing the composite Beam Pipe. First, the exact length of the Beam Pipe was determined by knowing the dimensions of the whole experiment. After determining the length, it was necessary to determine its diameter and wall thickness based on the required parameters. After the exact dimensions were already known, it was decided how many segments the whole Beam Pipe would consist of. After the final knowledge of the dimensions of the Beam Pipe, it was necessary to set the support positions in the space so that the pipe would not move freely within it. In the end, FEM calculations were performed to determine that the displacements from the vacuum and the actual load would be small enough that the Beam Pipe's deformation would not be too great.

5.1. Determining Beam Pipe basic dimensions

5.1.1. Length of the Beam Pipe

The origin of the coordinate system is in the target and in the direction of the beam or Beam Pipe is the Z axis. Because the Beam Pipe will tilt in the ± 2.5°, it is connected at the beginning to a tilting mechanism that is proposed in another Master's thesis [29]. As of today, it is still undecided which tilting mechanism will be chosen as the final one and therefore it is not possible to accurately determine the Z coordinate of the beginning of the Beam Pipe. Therefore, in this work, the longest tilting mechanism is calculated, where the point of contact is at $Z_{connect} = -4380\ mm$. At the end, there is a fixed wall that will have a beam dump built into it and the Beam Pipe will end in front of it. The distance of the wall from the target is $Z_{wall} = -20\,000\ mm$. In the end, there are two other limiting factors. One is the need to support the pipe at its end, and the other is the presence of a PSD detector with the furthest position $Z_{PSD} = -18\,300\ mm$. The construction, which will be used to support the Beam Pipe in the end will need the space around it. For this reason, the most distant position of the Beam Pipe will be on the coordinate $Z_{end} = -19\,000\ mm$. From the difference between the coordinates, the total length of the pipe was determined:

$$L = Z_{end} - Z_{connect} = 19\,000 - 4\,380 = 14\,620\ [mm] \tag{24}$$

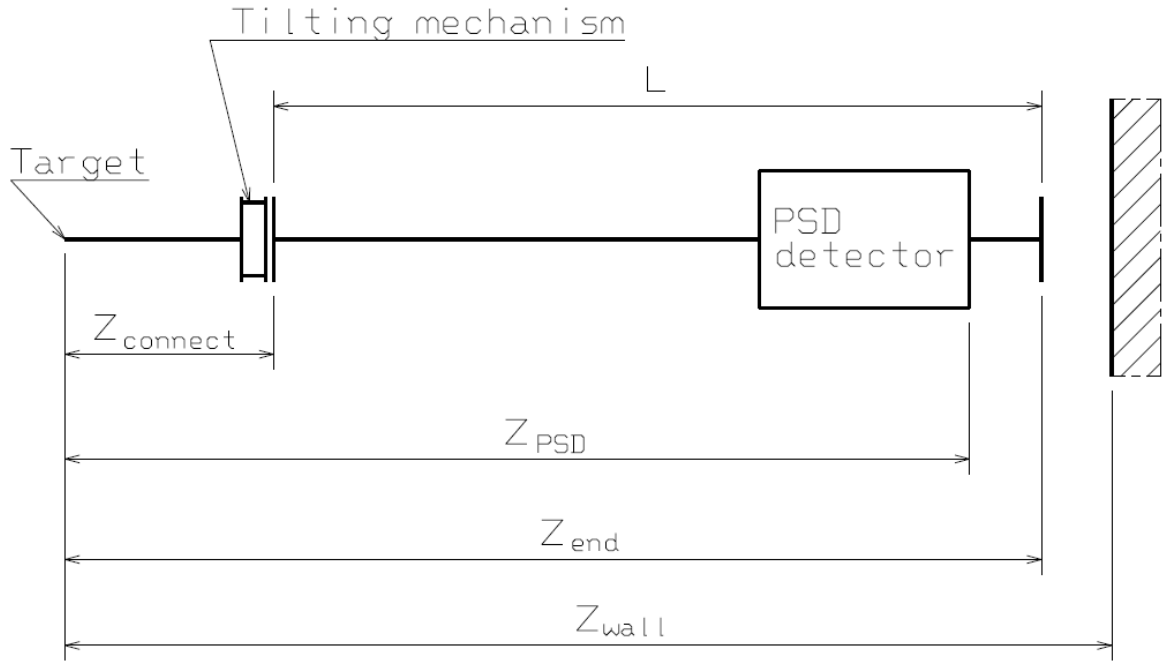

Figure 27: Overview of Beam Pipe

5.1.2. Diameter of the Beam Pipe

The diameter should be as large as possible. The limiting parameter for the diameter is the passage through the PSD detector. The PSD detector consists of several PSD modules, each with a mass of about 500 kg. There are 2 ways in which PSD modules will be stacked together in a PSD detector. For the first one, shown in Figure 28 a), the problem does not arise because PSD modules are not allowed to move downwards because of their arrangement. But if the PSD modules are in a configuration as shown in Figure 28 b), then the problem is already present. It's evident from this figure that there is nothing to stop the PSD modules from moving downwards. The dimension of each of them is 200 x 200 mm and some parts will have to be inserted into the empty space in the middle of the PSD detector to prevent PSD modules from moving. The solution to this problem is in chapter 5.6, however it can be said that the hole through which the Beam Pipe has to pass the beam is 190 x 190 mm.

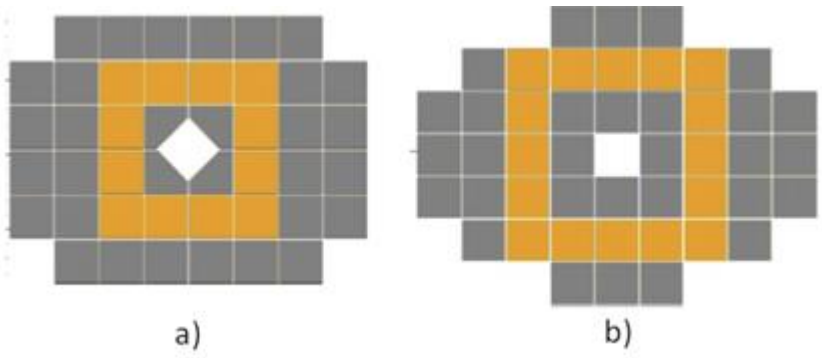

Figure 28: Configurations of PSD detector

Since multiple different types of segment connections are proposed, for simplicity it is assumed that for each type of connection the Beam Pipe diameter will be the same. The

largest type of connection is the flange. Its design gives us a maximum Beam Pipe diameter of 180 mm. Determining wall thickness was tentatively designed to be 2 mm. A smaller wall thickness could pose problems in the form of a small bending stiffness or tendency to delaminate. Greater thickness is also undesirable given the material budget.

5.1.3. Wall thickness

Because the Beam Pipe will be tilted, its movement must be controlled. In the thesis [29], the tilting mechanism and its control is designed. One way to control the movement of the whole Beam Pipe was with a PSD detector. The PSD detector has its own drive, so from that standpoint, it's a possible solution. While this was a considered possibility, a tilting mechanism with a large bellow was being considered. The bellow tends to return to its initial position under vacuum in the tilted position, and the Beam Pipe would have to overcome this resistance. This leads to its bending. This situation and the determination of the minimum wall thickness is shown below.

The Beam Pipe will be most stressed when the PSD is in the position furthest from the tilt mechanism. The force created on the bellow, which will create a bending moment is 163 N in the unloaded state, and if the air is extracted, the force will increase to 3500 N [29]. In fact, the Beam Pipe must overcome this moment with its entire length. In addition, if the Beam Pipe bends too much, the beam will not be able to pass. This means that it is necessary to find such a wall thickness that the Beam Pipe deforms only enough so the particles can pass through.

It is first necessary to determine how much the axes of the deformed and undeformed pipes can rotate relative to each other for the beam to pass. This depends on the wall thickness, because if the wall thickness increases, the inner diameter of the pipe decreases and thus the difference in rotation. Catia software was used to determine this parameter. A parametric model was created and decreasing the diameter reduced the difference in rotation, which was measured for several different thicknesses with results presented in Table 5.

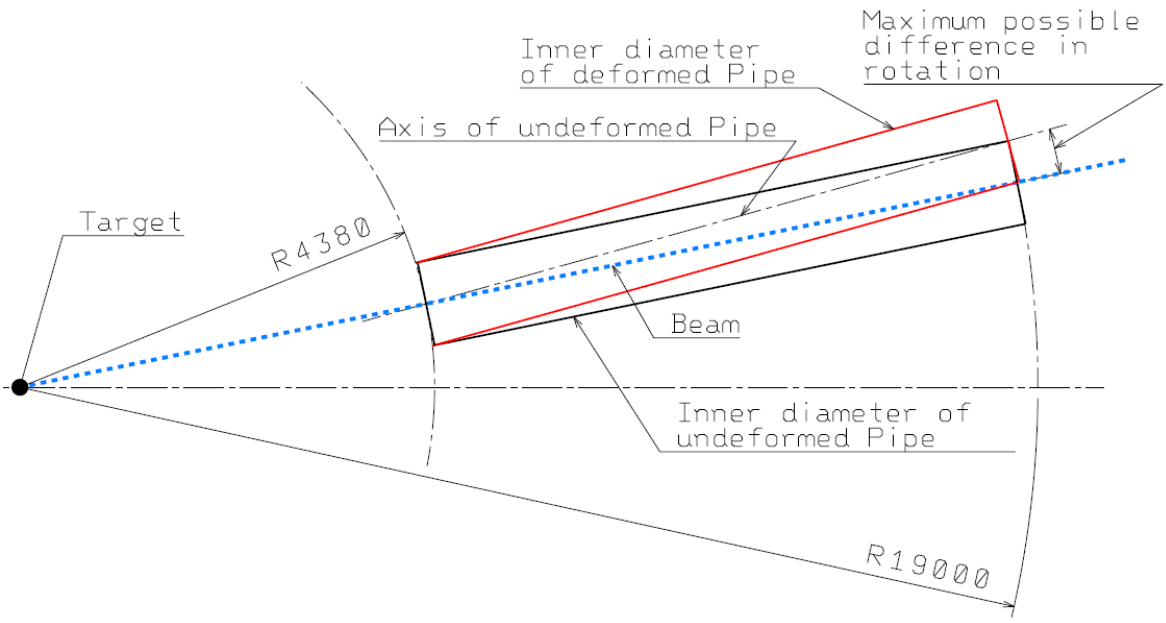

Figure 29: The schematic view of tilted Beam Pipe with deformed and undeformed Pipe

The next step was to set up the model in Ansys. A long tube was made and embedded at its end at a length of 1650 mm, as in the PSD detector. The result was a deformation in the x, y directions and these were then converted to a difference in rotation, which is the final result. This measurement was performed for different wall thicknesses with loads of 163 N and 3500 N, respectively.

The results are presented in Table 5, from which graphs were then made and are shown in Figure 30 and Figure 31. It is clear from the results that it is not possible to control the tilting of the Beam Pipe using a PSD detector without using a control mechanism on the bellow, because the Beam Pipe would be deformed too much. In fact, the Beam Pipe would not even achieve such deformations, but would be destroyed.

Table 5: Results of allowed differences and results of difference in rotation from Ansys

Wall thickness [mm]	Difference in rotation with vacuum load [°]	Difference in rotation without vacuum load [°]	Maximum possible difference [°]
1	63.500	2.946	0.283
2	32.171	1.498	0.280
4	16.648	0.775	0.274
8	8.916	0.415	0.261
12	6.371	0.297	0.248
16	5.121	0.239	0.236
20	4.400	0.204	0.223
32	3.373	0.157	0.185
40	3.088	0.144	0.159
48	2.937	0.137	0.134

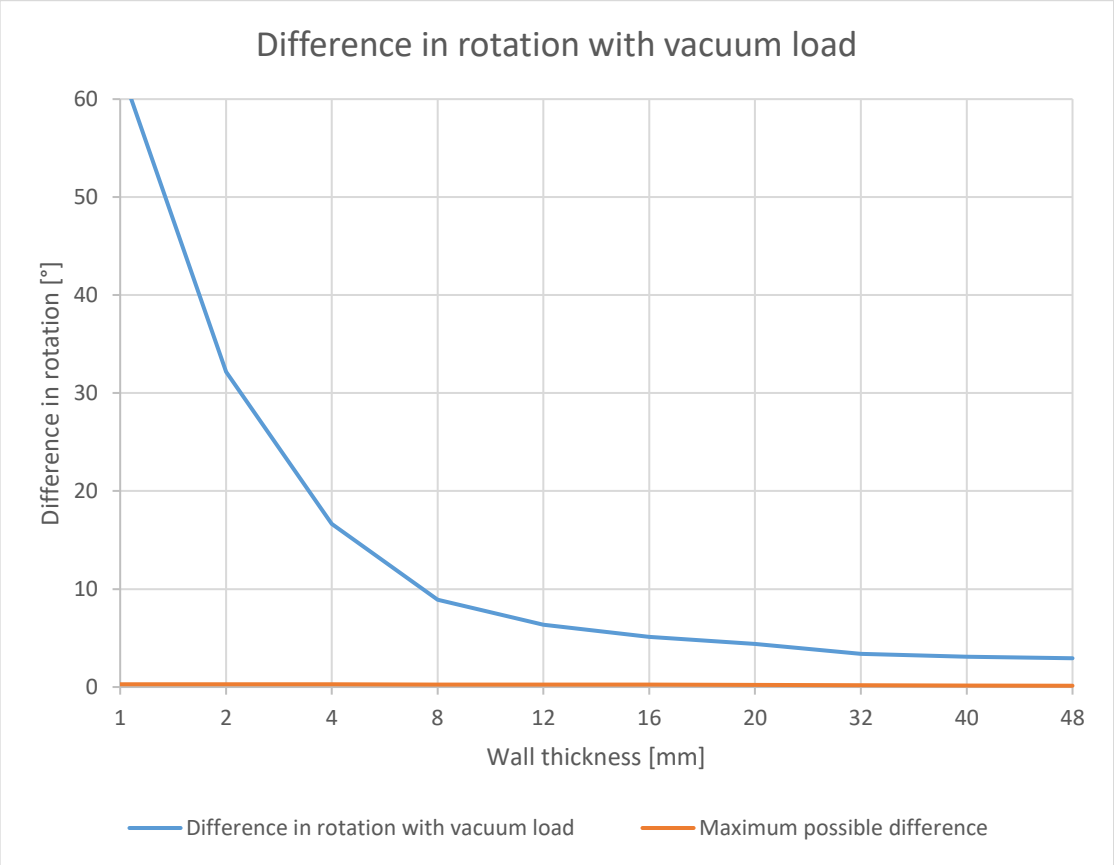

Figure 30: Difference in rotation with vacuum load

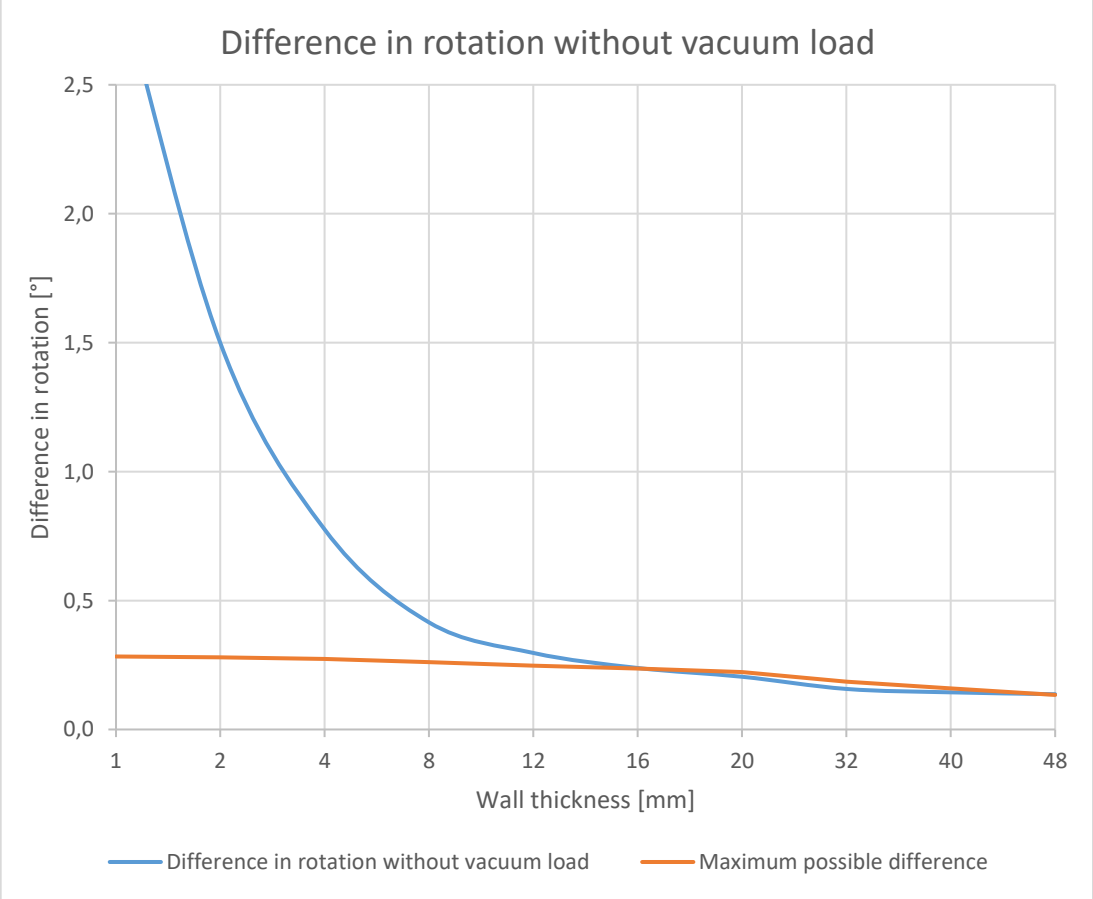

Figure 31: Difference in rotation without vacuum load

5.2. Connections

The Beam Pipe has a total length of 14 920 mm and because it will be divided into modules it needs to be connected appropriately. Chapter 5.6 shows that the maximum connection size is a 190 x 190 mm square. Several types of pipe connection were created in the construction, from which the two best-performing variants were selected. For both means of connecting the modules, FEM analysis was performed to determine the maximum deformation.

5.2.1. Slide-in connection

This type of connection has been made in several different variants and can be redesigned even now. Slide-in connection is a way of connecting without using screws, and metal materials altogether. Vacuum tightness is provided by O-rings. The Beam Pipe will most likely be produced by the winding filament method, which is the appropriate production method for this type of connection. The Beam Pipe has the same outer diameter of 180 mm along its entire length. A larger diameter is wound at both ends to allow O-rings grooves to be made into the tube, but it must not be lower than the diameter that is the Beam Pipe's outer diameter. Once the pipes are in place and are already fitted with O-rings, a connection pipe will be mounted over them to ensure connection and vacuum tightness. There is no element in this design that would prohibit the movement of the connection pipe, and the movement is thus restricted only by the pressure that is produced by the compression of the O-rings. However, this pressure is large enough to keep the connection pipes from moving. This type of connection is shown in Figure 32, Figure 33 and Figure 34.

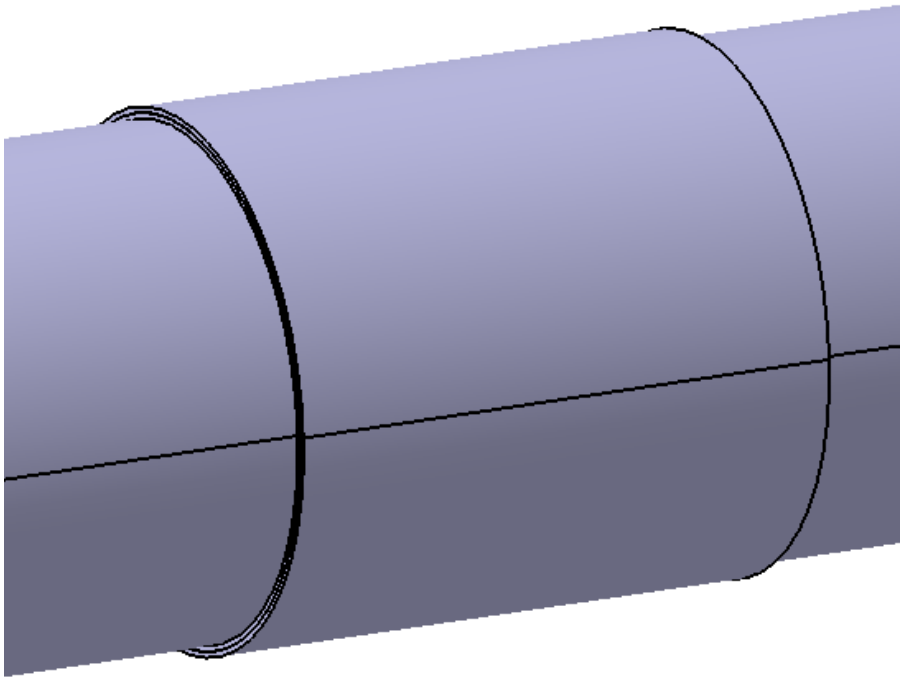

Figure 32: Slide-in connection

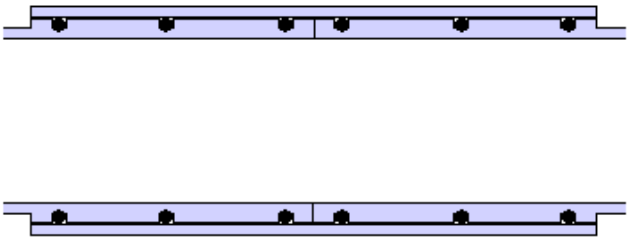

Figure 33: Section cut of slide-in connection

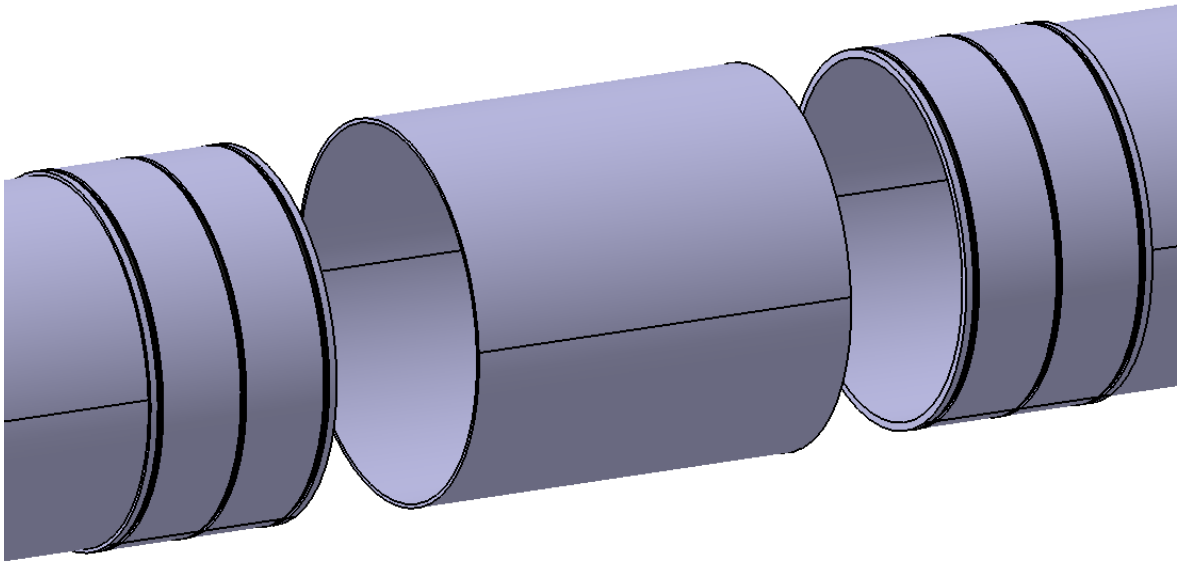

Figure 34: Disassembled slide-in connection

This solution makes it possible to dismount any part of the Beam Pipe independently of others. Simply move the connection pipe at both ends to the side and remove the piece of pipe. Also, one side could be fixed with the connection pipe, e.g. by gluing. Then only three O-rings would be needed, and the Beam Pipe will have to be mounted in predefined order.

5.2.2. Flange connection

This type of connection needs more material than the previous solution but it is necessary because the tilting mechanism will be connected by Beam Pipe in this way. In this case, the pipes will be made with the same diameter throughout and flanges will be fixed to its ends, e.g. by gluing. The flanges could be made of any material. PEEK (Poly-ether-ether-ketone) is a suitable choice of material to meet requirements. The flange is square-shaped because of the hole it has to pass through the PSD detector and its shape does not change, because of the economy. The flange connection will allow any part of the pipe to be disassembled without the need to other segments. Vacuum tightness is ensured on the front surfaces of the flanges and the connection is ensured by four screws, where one of the flanges has a groove for the O-ring and the other flange has a straight front face. Details of the connection are shown in the figures below.

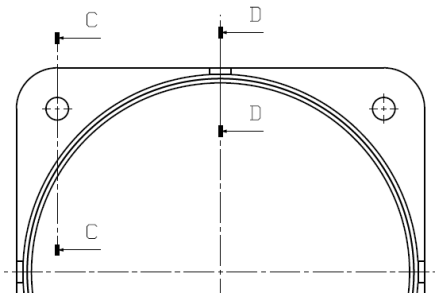

Figure 35: Position of section cuts

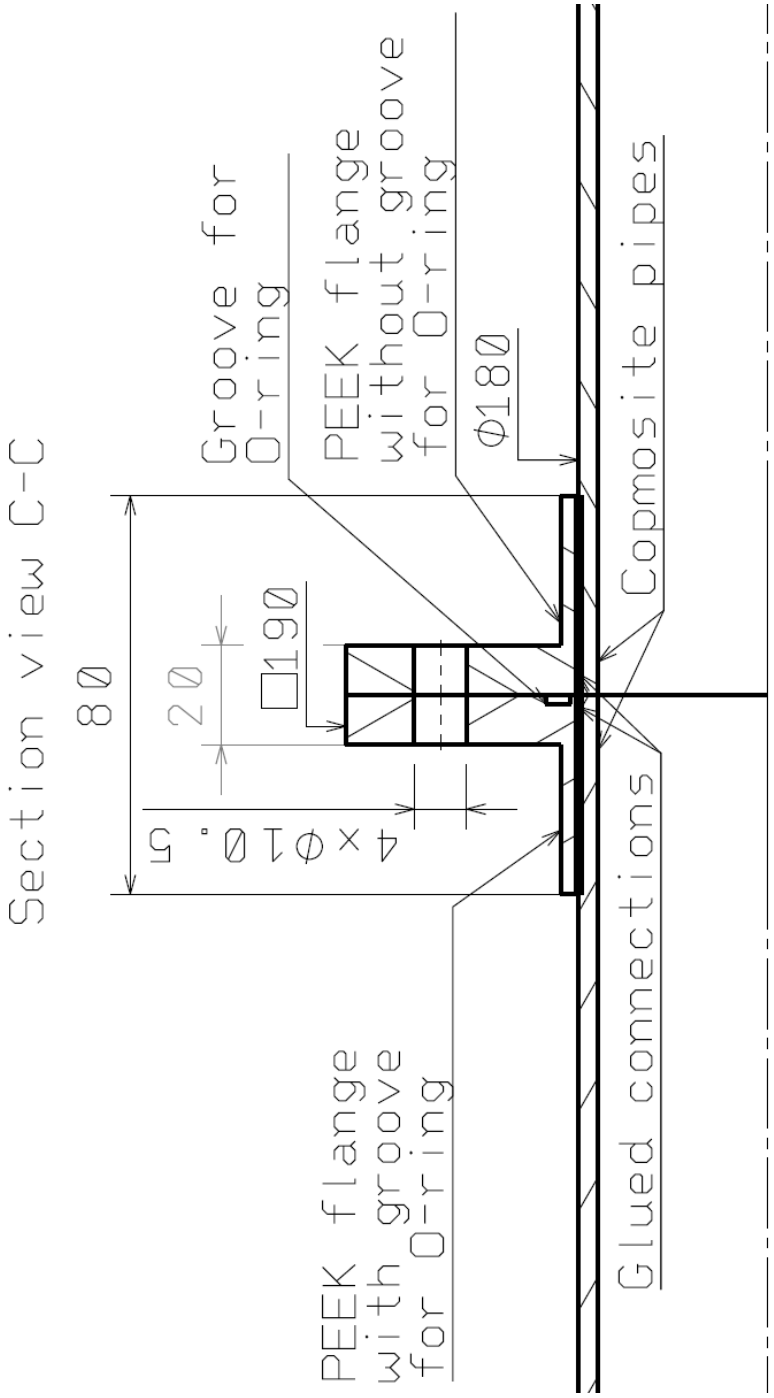

Figure 36: Section cut C-C

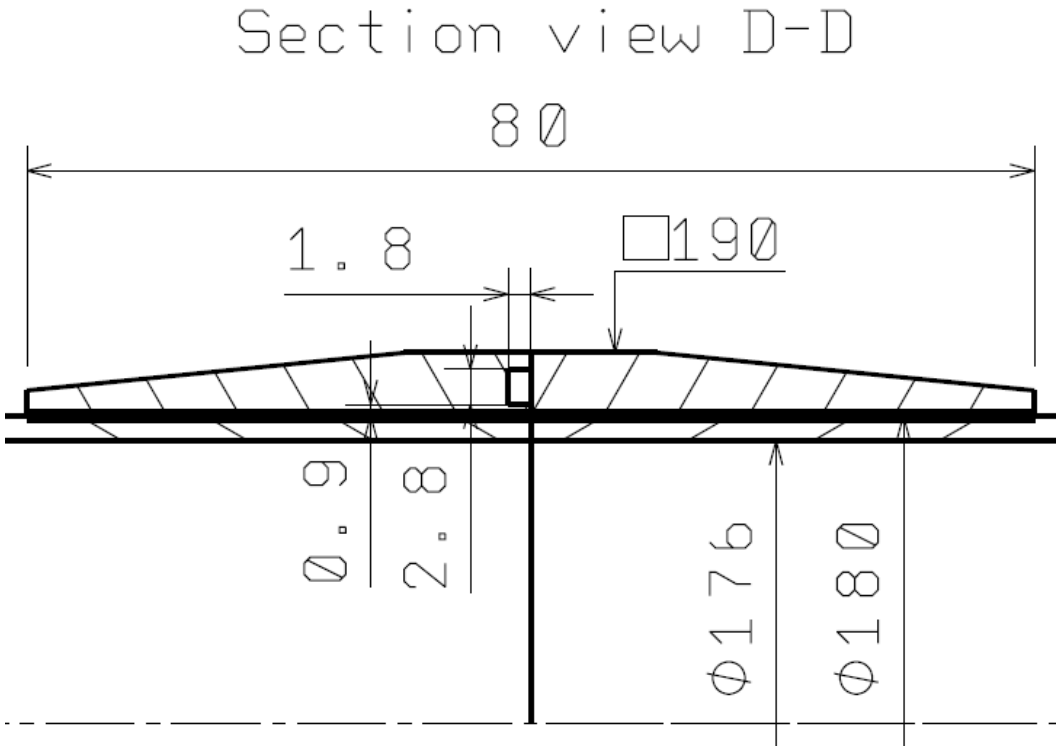

Figure 37: Section cut D-D with detail of groove for O-ring

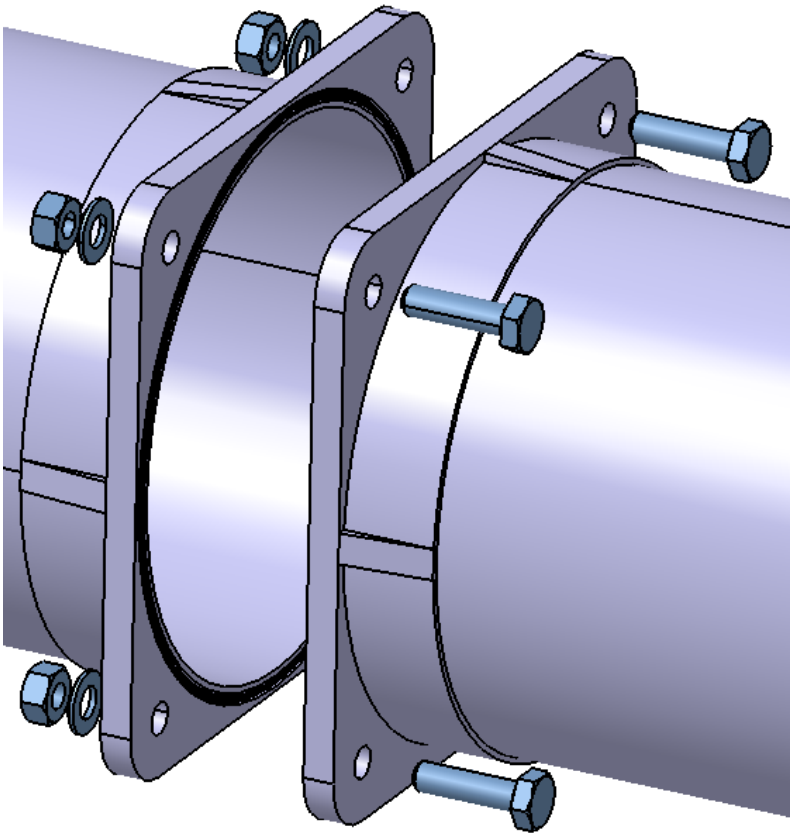

Figure 38: Disassembled flange connection

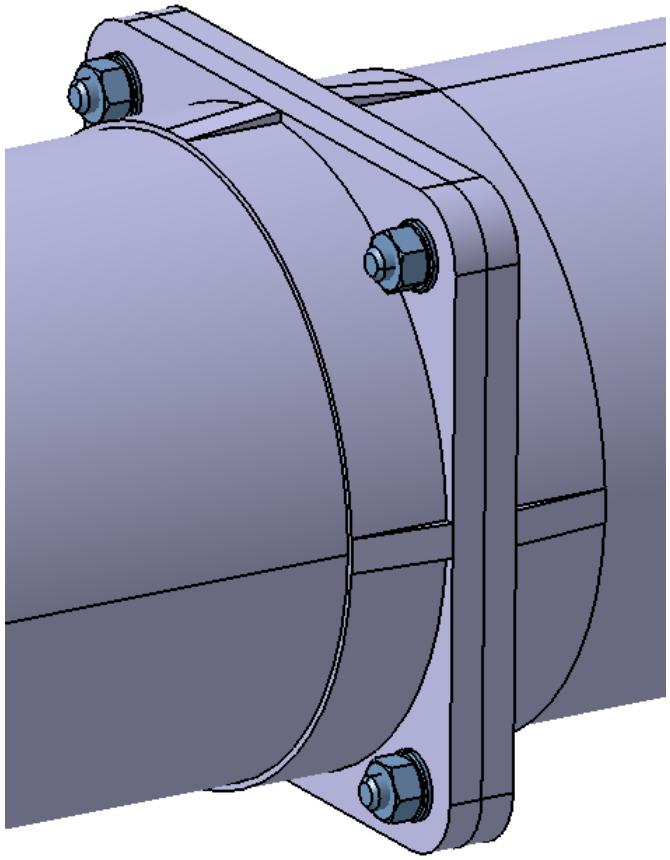

Figure 39: Flange connection

5.2.3. FEM Analysis of connections

Both types of connections were set in the same way. In the Ansys, the composition of the composite pipe from the four layers was set up by the ACP module. The overall wall thickness is 2 mm so one layer is 0.5 mm. The composition was chosen +45°/-45°/+45°/-45°. The goal was to figure out what the Beam Pipe maximum deformation will be and how the Beam Pipe will deform and the behaviour of individual layers using Inverse Reserve factor. Failure is experienced when an Inverse Reserve Factor is greater than 1.

A single connection has been made to the Beam Pipe at its centre, because that's where the greatest bending moment will be. A situation is considered where axial force is not carried by the pipe. The greatest bending moment will be at the greatest length, so two tubes with a length of 7 310 mm have been created. At the end, where the tilting mechanism is, the Beam Pipe is fixed. At the other end, where it is enclosed by a cap, only movement in the axial direction is allowed. Moreover, the pipe contains vacuum resulting in pressure on the outer surface.

For the slide-in connection, the maximum deformation is 2.81 mm. So the deformations are not large, but if we want to reduce them further, it will be necessary to

create a support. There should be no failures, because the Inverse Reserve factor is less than 1 along the entire length.

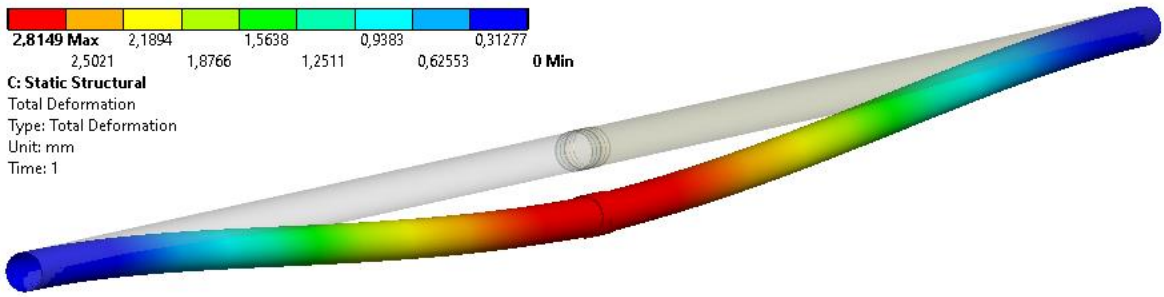

Figure 40: Total deformation of Slide-in connection

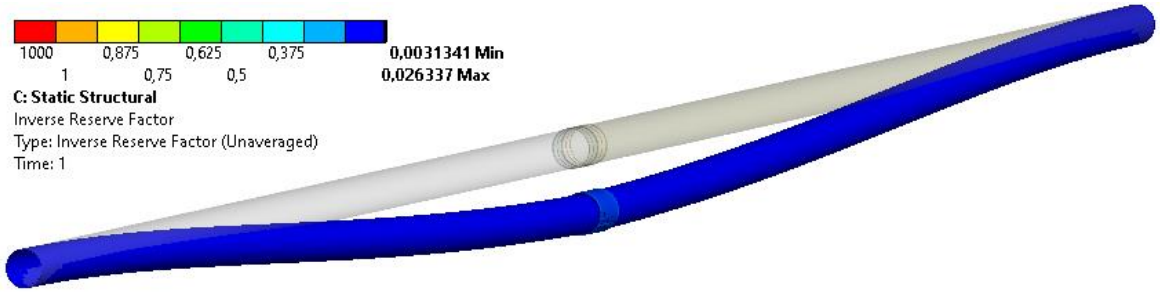

Figure 41: Inverse reserve factor of Slide-in connection

PEEK flanges are considered and are bonded with the pipes. The maximum pipe deformation with flange connection is 2.41 mm. That's less than in a case with slide-in connection, which means the connection is stiffer. Inverse Reserve factor is less than 1, so no failure will happen.

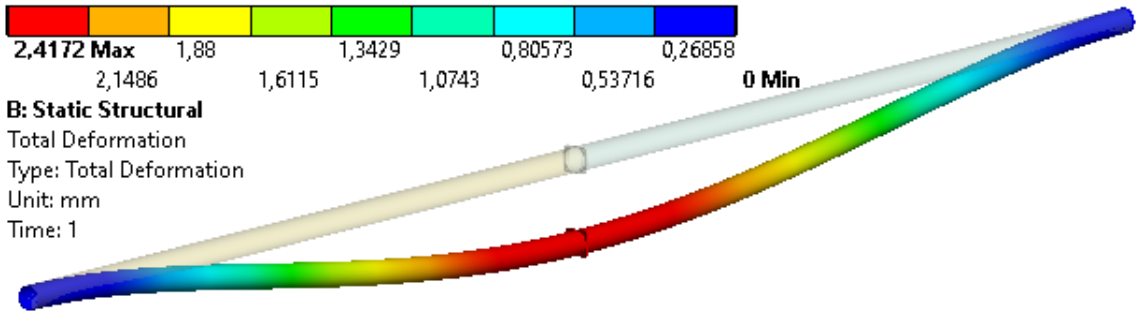

Figure 42: Total deformation of Flange connection

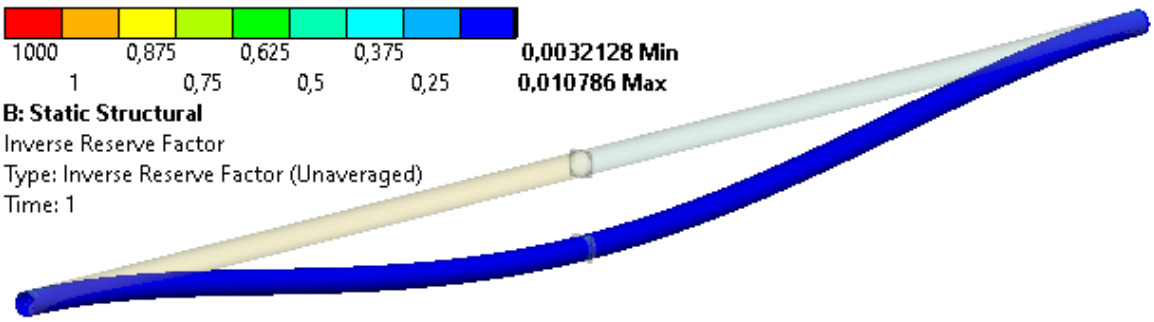

Figure 43: Inverse reserve factor of Flange connection

5.3. Modules

The Beam pipe consists of several modules that are presented on the following pages.

The first piece of the Beam Pipe is a pipe with flanges at both ends. On the end where the Beam Pipe is connected to the tilting mechanism there is a flange, so there will be a flange on the first tube too. There is also a flange at the other end to make the first piece of the Beam Pipe easily removable if necessary. The first piece is shown in Figure 44 and Figure 45.

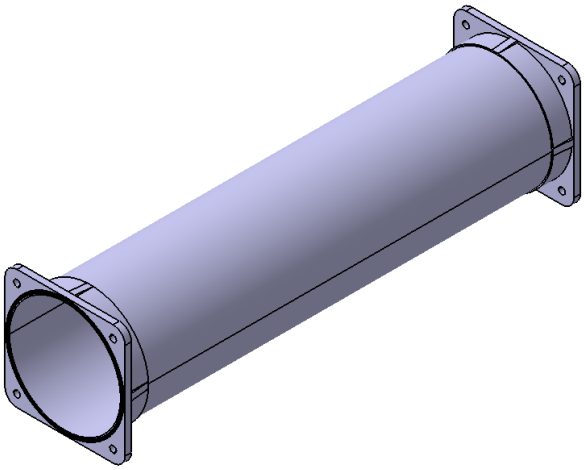

Figure 44: First piece of Beam Pipe

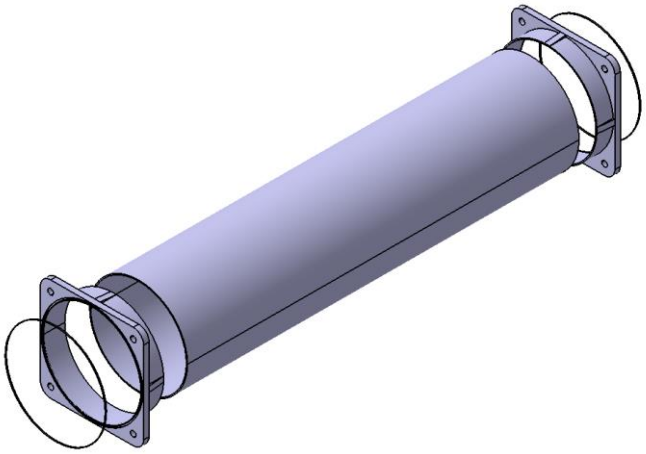

Figure 45: Disassembled first piece of Beam Pipe

Next is a piece that serves as a transition between the flange connection and the slide-in connection. This means that on one side it is fitted with a flange and on the other side the pipe is wound with a larger diameter with grooves for the O-rings. In addition, the ISO-KF flange intended for vacuum input or measurement can also be seen.

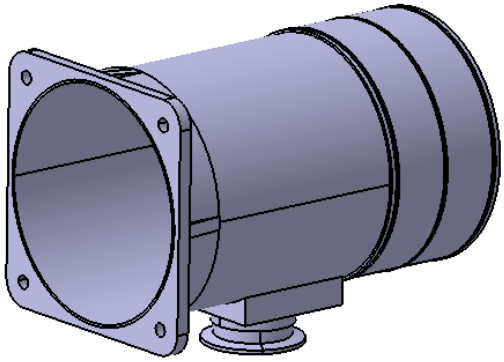

Figure 46: Transition piece of Beam Pipe

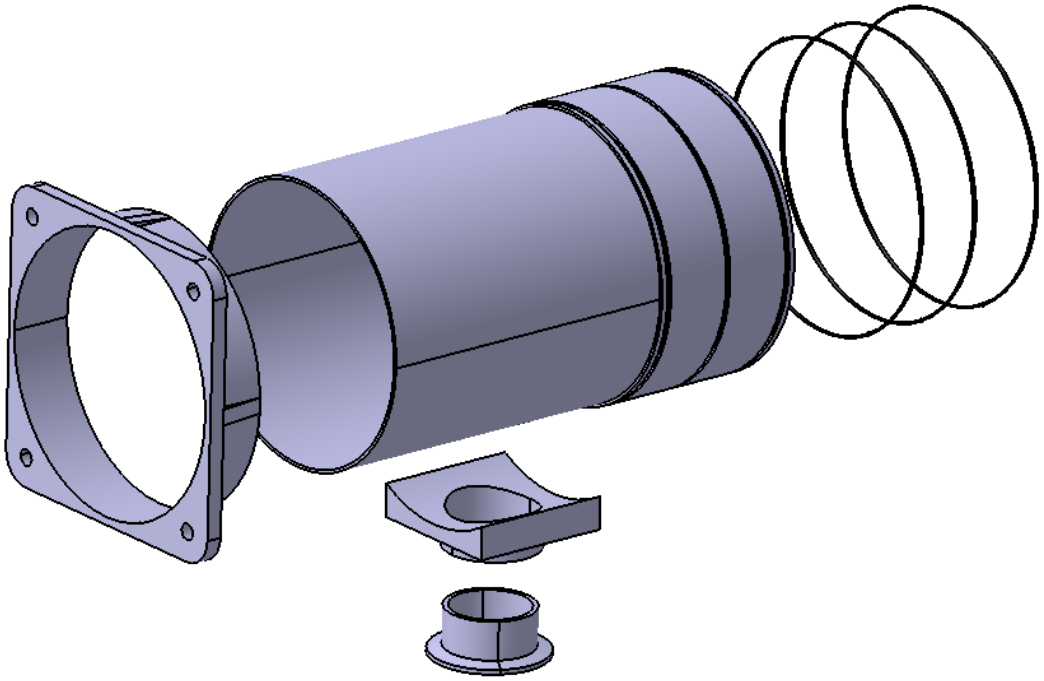

Figure 47: Disassembled transition piece of Beam Pipe

This piece can appear in several places on the Beam Pipe, depending only on the position where a vacuum input is needed. If not required, they can be removed from the Beam Pipe. The vacuum inlets are in short pieces so that they can be put in different positions on the length of Beam Pipe. In fact, there may be a configuration of the experiment that prevents the presence of an ISO-KF flange at some point.

The module shown in the Figure 48 is the longest of all the other parts. The maximum length of one segment is 5 m, according to the specification, this pipe is 3 metres long. In the manufacture of composite tubes by winding, the most expensive product in the entire manufacturing process is the mandrel, which is why the segment length of 3 metres has been chosen. A detail of the end of the pipe is shown in Figure 49.

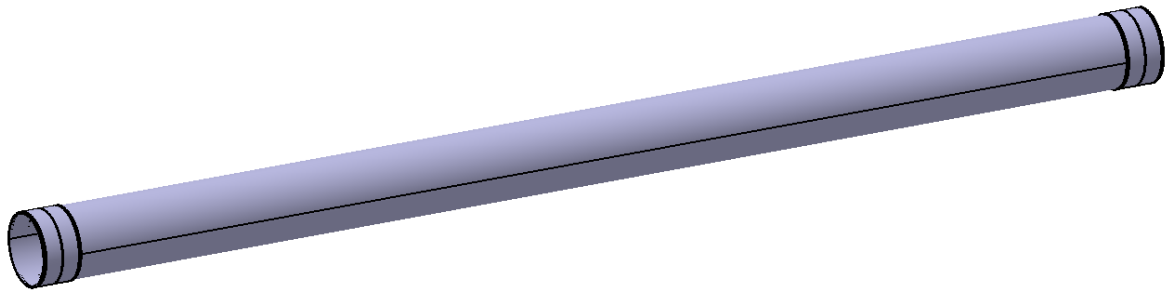

Figure 48: Long part of Beam Pipe

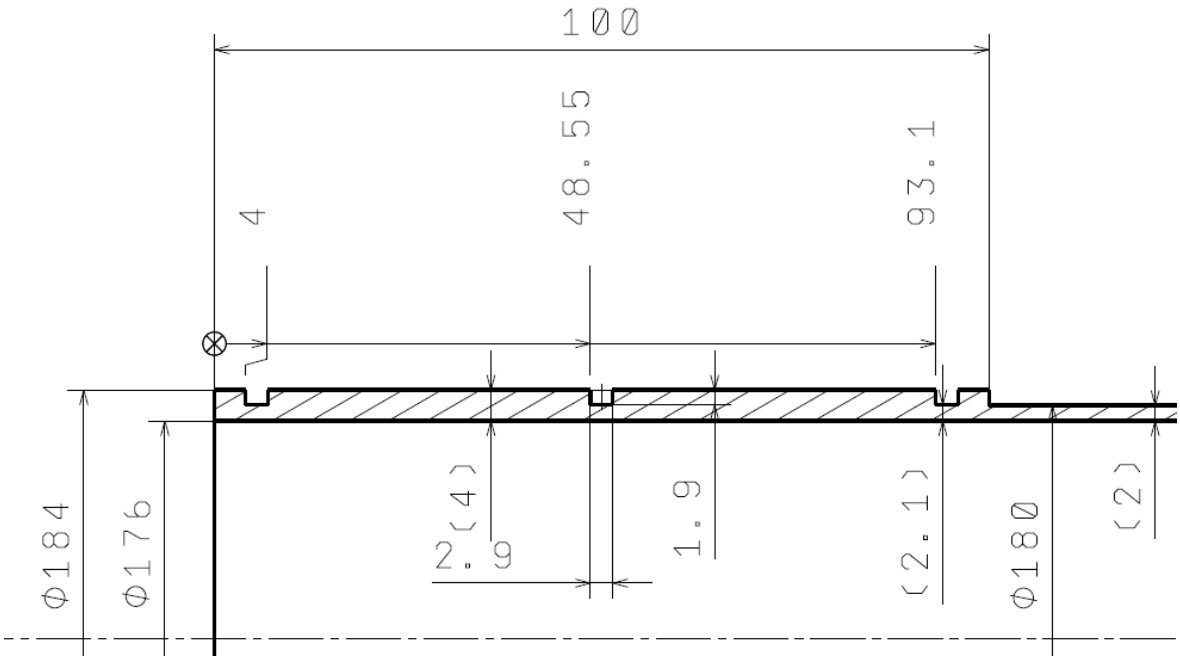

Figure 49: Detail of end of long Beam Pipe part

The final element of Beam Pipe is the cap that closes it. The cap is designed to be fixed to the frame to hold it in a defined position. This piece consists of a flange, a short tube and a cap with ISO-KF flange for vacuum input. The short pipe is glued into the flange and the vacuum tightness is ensured by slide-in connection. The flange is a massive part to allow the attachment of the cap and the frame to eliminate the axial force produced by the vacuum. The two holes at the bottom serve for a fixed connection to the pin, which is further connected to the mechanism defining the movement of the Beam Pipe end. There is a screwed cap on the flange with a vacuum inlet and vacuum tightness is ensured by the use of an O-ring. The ISO-KF flange is welded with the cap.

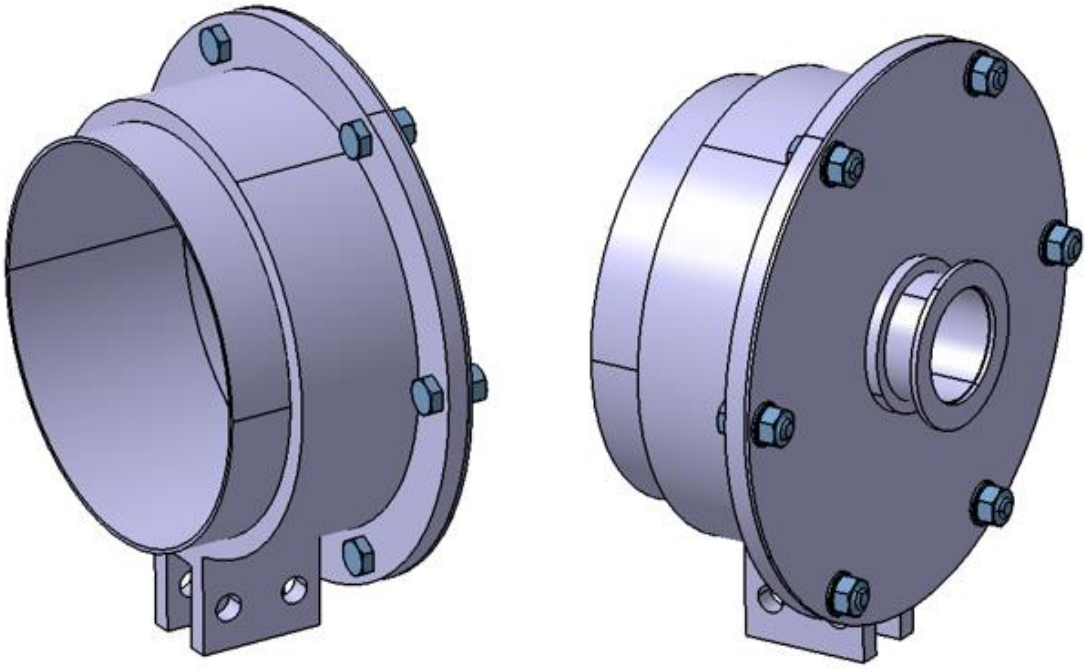

Figure 50: Beam Pipe's cap with vacuum input

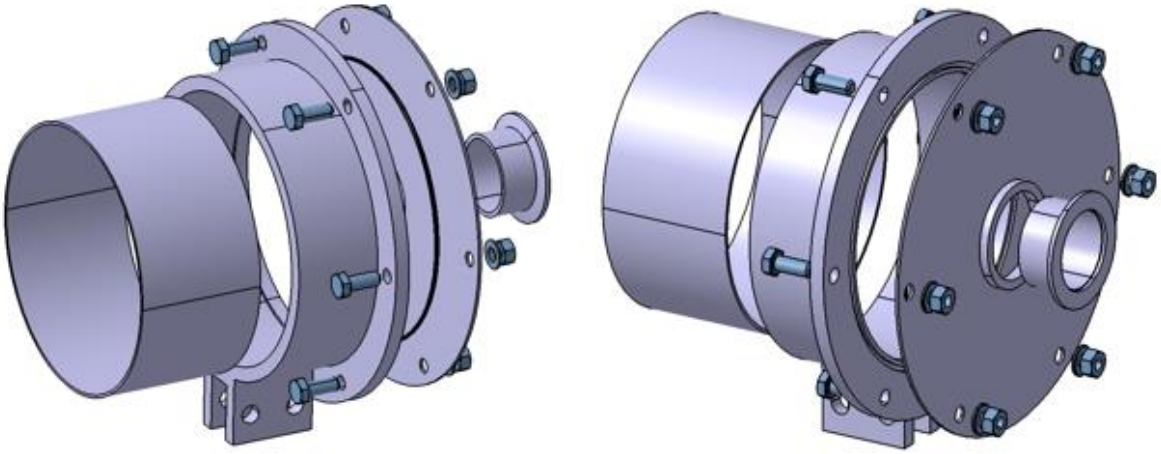

Figure 51: Disassembled Beam Pipe's cap with vacuum input

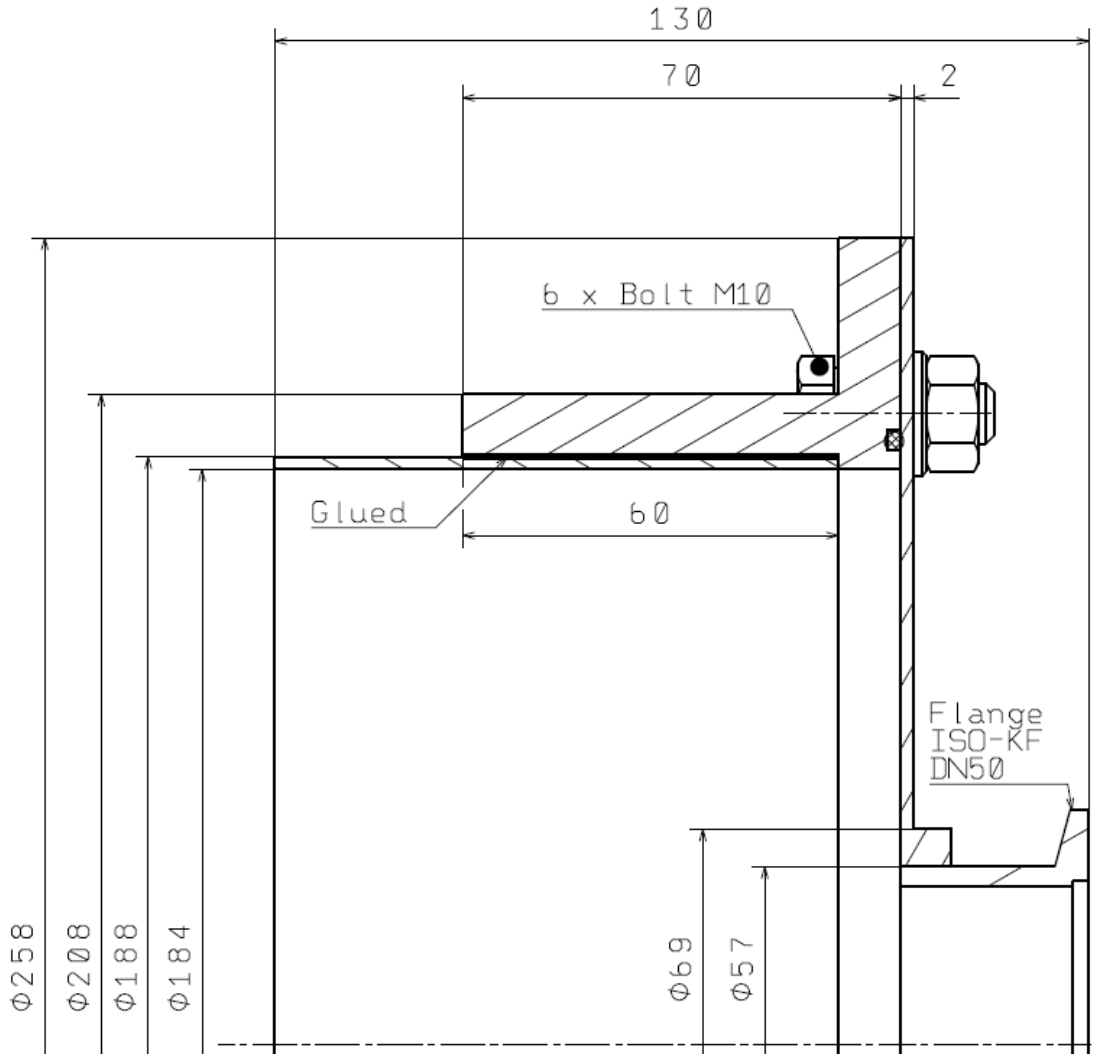

Figure 52: Section cut of Beam Pipe's cap

5.4. Vacuum inputs

Two possible solutions have been proposed for vacuum inputs. Both options include an ISO-KF flange, which is standardised and can be purchased. One option, is to prepare the pipe for a tube cylindrical outlet into which a vacuum flange can be fitted, as shown in Figure 53. The second way of connecting the vacuum input requires an additional part. This part can be made from stainless steel, aluminium or PEEK and can be joined with the ISO-KF flange by welding or gluing. Next, it can be added to the pipe by gluing, or it could be wrapped with carbon fibres in the manufacture of the pipe itself, as shown in Figure 54. The former is more material-efficient, but is more manufacturing-complex than the latter, so these aspects need to be considered carefully when making a final choice.

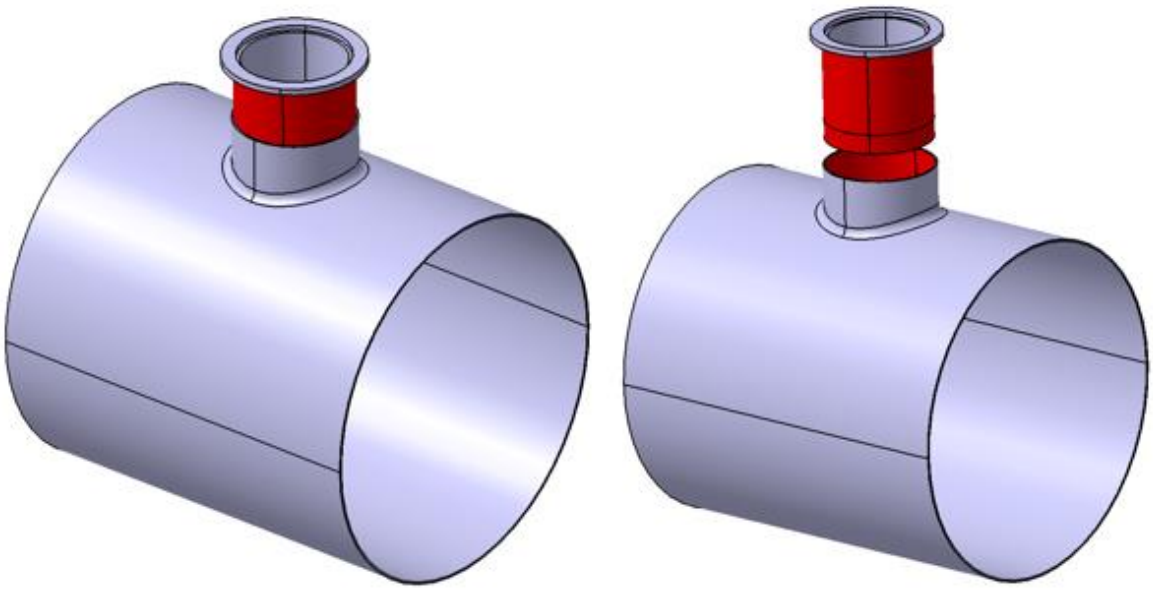

Figure 53: Vacuum input with cylindrical outlet on pipe

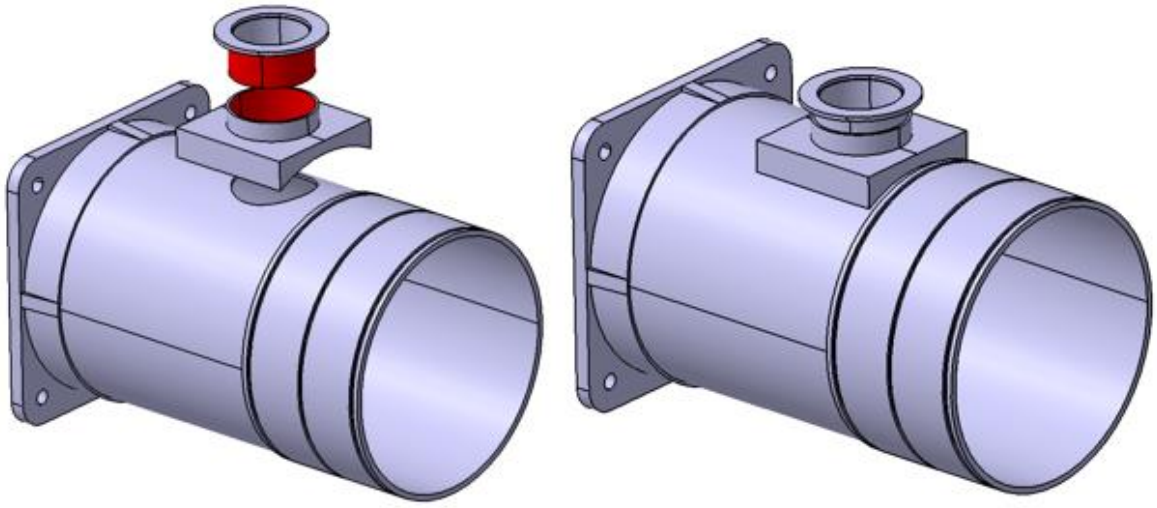

Figure 54: Vacuum input with extra part

5.5. Supports

The Beam pipe must be supported somewhere along its length, but the position of the detectors and their movements make it impossible to make static support, except for the end position. Therefore, for supports in the middle of the Beam Pipe, a space will have to be defined in which support could be created, or support will have to be attached to one of the detectors.

The support could be sliding on rails that are on the ground, but since the Beam Pipe is 5 metres high, the construction could be relatively large, which is undesirable. If the support is mounted directly on one of the detectors, and at the same time the configuration of the experiment changes under the vacuum, then the Beam Pipe would have to move freely in the support in axial direction. Two conceptual designs were made and using rollers. The variant shown in the Figure 55 on the left is not suitable for flange connection.

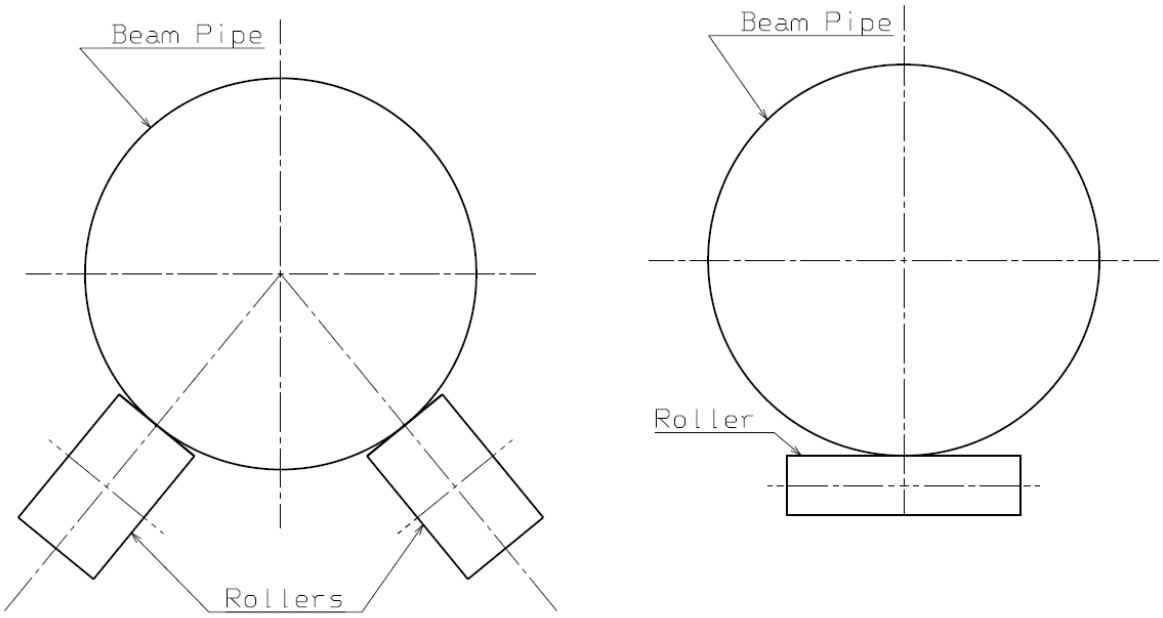

Figure 55: Concepts for Beam Pipe's support

If the support is in contact with the connection, it would have to be adjusted accordingly. This will not be a problem for connecting with the flanges, as a tilted plane will be made to slide the roll down. For a slide-in, runs would also have to be made for a larger diameter. If the rolls had a big enough diameter, the smaller diameter differences that are on the connections should not matter at all. Both situations are in Figure 56 for flange connection and in Figure 57 for slide-in connection.

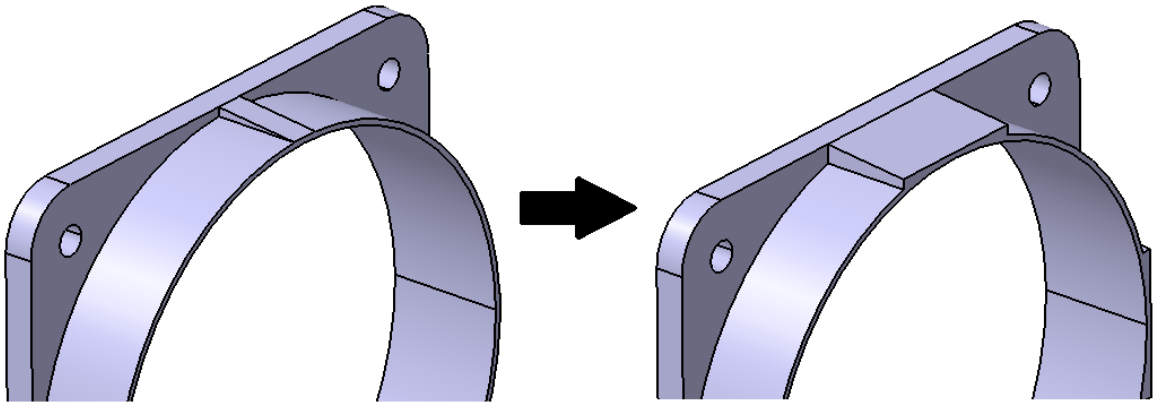

Figure 56: Flange connection modification for support with rollers

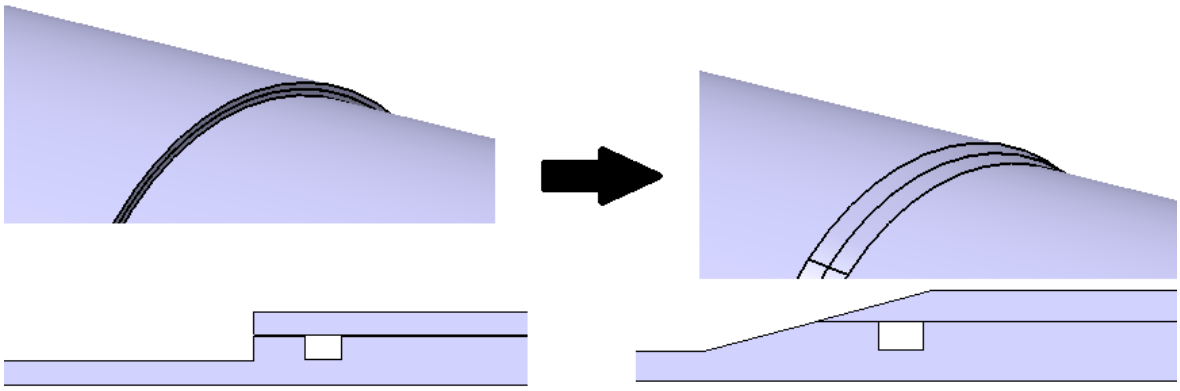

Figure 57: Slide-in connection modification for support with rollers

At the end of the Beam Pipe, it needs to be in a well-defined position. This can be achieved by a mechanism to which the cap will be firmly attached. Requirements to save material behind all detectors are no longer so strict, so the construction could be more massive. Arch movement will be ensured using a curved guide system that can use either rolls or bushings. It is first necessary to know the dimensions of the arc along which the mechanism will move, which will be determined as follows:

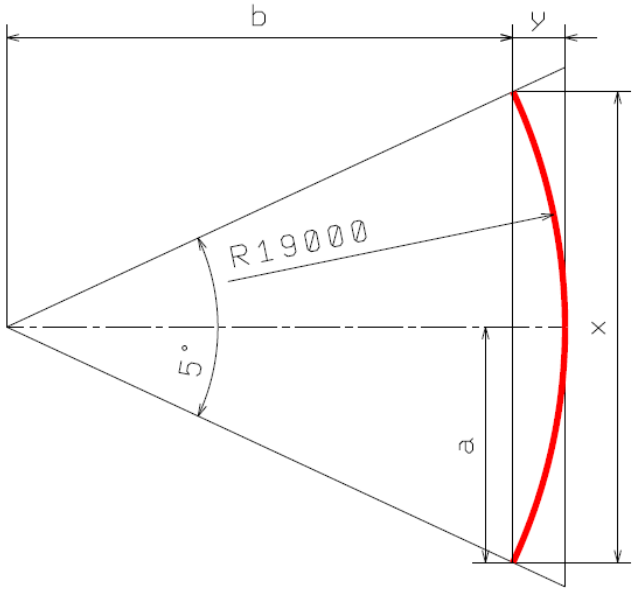

Figure 58: The schematic view of motion of Beam Pipe

$$a = \sin(2.5) \cdot 19\,000 = 828.77\ [mm] \tag{25}$$

$$b = \cos(2.5) \cdot 19\,000 = 18\,981.62\ [mm] \tag{26}$$

$$x = 2 \cdot a = 2 \cdot 828.77 = 1\,657.4\ [mm] \tag{27}$$

$$y = R - b = 19\,000 - 18\,981.62 = 18.08\ [mm] \tag{28}$$

Another possibility is that the Beam Pipe will be tilted by two drives. One in the PSD detector and one on the tilting mechanism, so only the support at the end of the Beam Pipe ensures movement along an arc. However, if controlling of the end of the Beam Pipe were to be required, then it can be connected to the controlling mechanism. Figure 59 shows the combination with the controlling mechanism. The axis of the yellow pin is perpendicular to the arc on which the Beam Pipe moves. In the red part, the pin is supported by bearings so that it can rotate. The red part is connected by green rods to the blue mechanism, and they must be supported freely in the axial direction. In the blue part, a mechanism is needed to control the linear motion, so it is possible to use a lead screw powered by a stepper motor, for example.

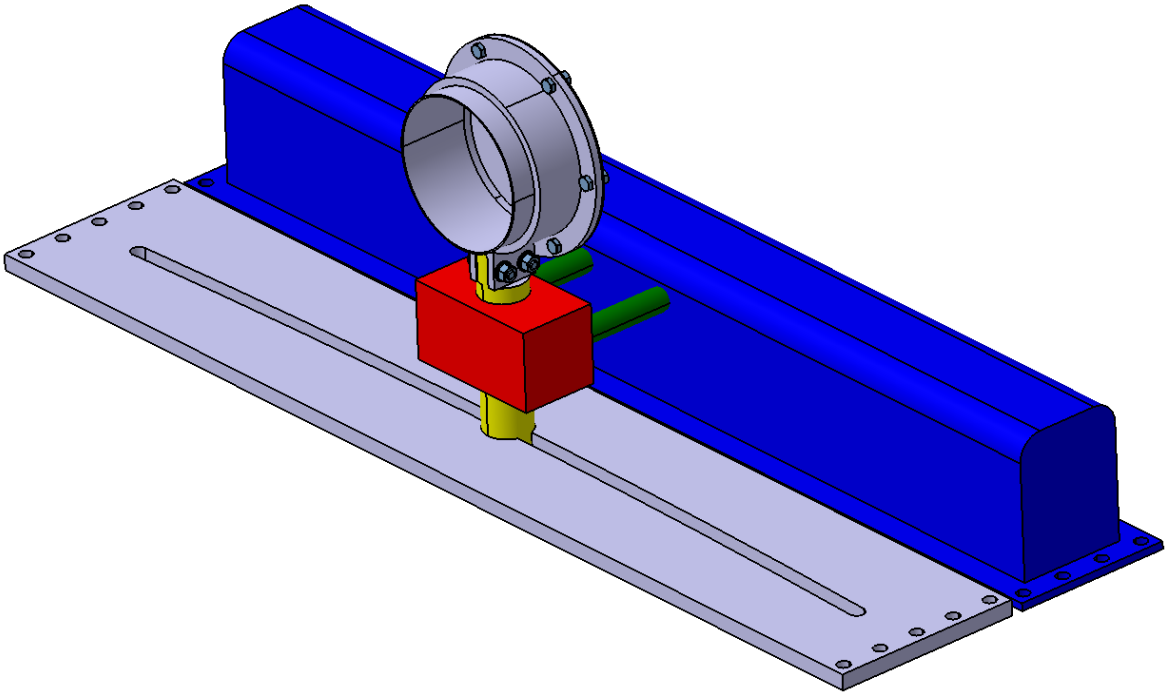

Figure 59: End cap with controlling mechanism

As has been said, one way of defining arc movement is the bushing it is supposed to travel on. The yellow pin is shaped on the underside to fit perfectly in the groove. If this support also serves to carry the axial force generated by the vacuum, there is a screwed-in plate on the underside to carry the bending moment, as shown in Figure 60

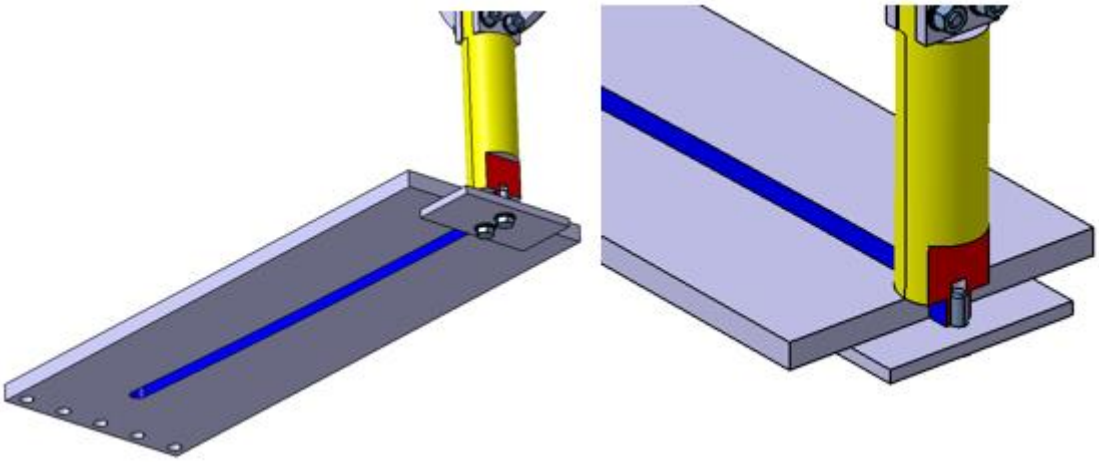

Figure 60: Arc groove defining motion of Beam Pipe

Another possiblility is to use rollers. The plate is attached to a fix frame using a series of screws and is shaped like an arch to move along. The shape of the rollers also ensures that the resulting bending moment is captured. A bolt with a cap may be welded to a board that moves, or another method of connection may be chosen. This way is shown in Figure 61, Figure 62 and Figure 63. More similar rail systems exists, but for production in the required dimensions, this is the simplest solution.

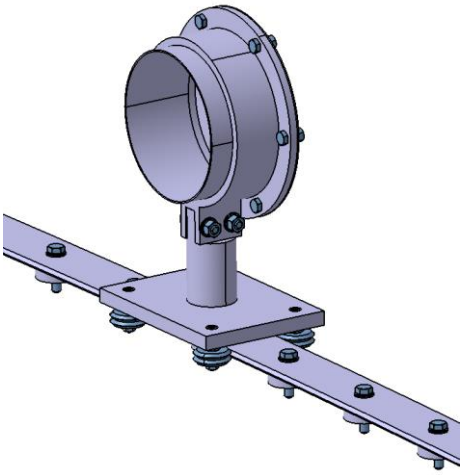

Figure 61: Roller system defining motion of Beam Pipe

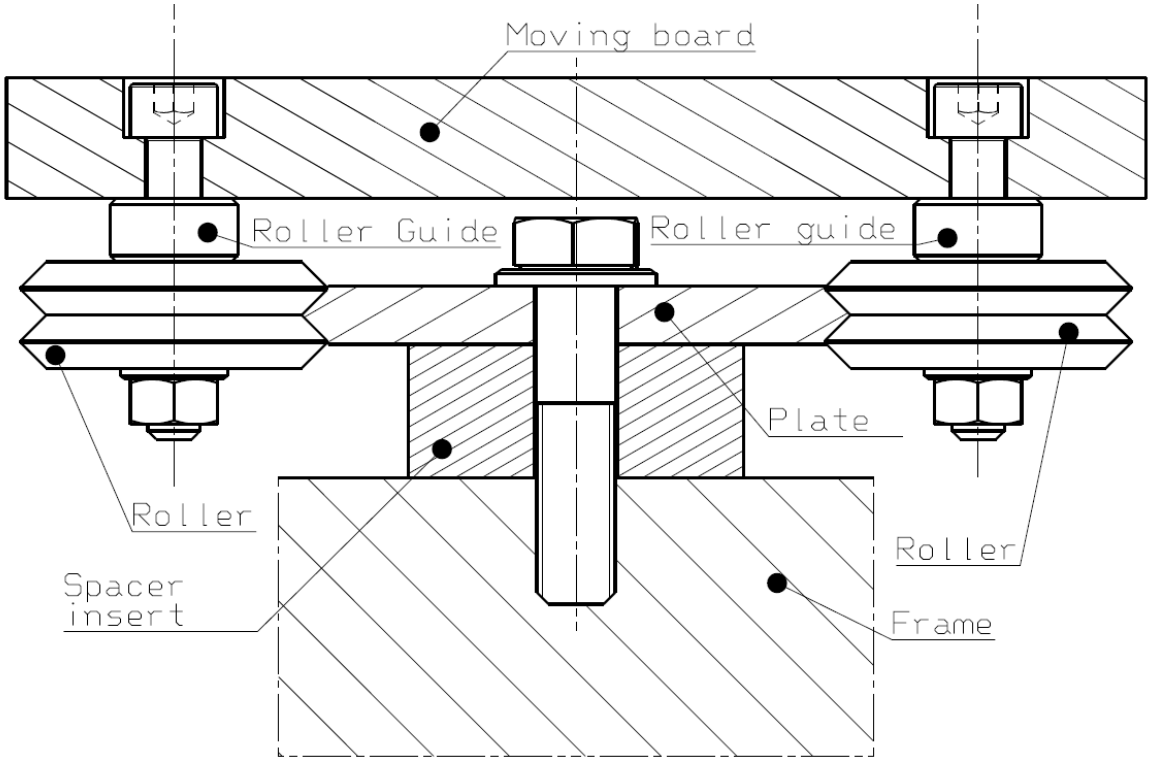

Figure 62: Section cut of roller system defining motion of Beam Pipe

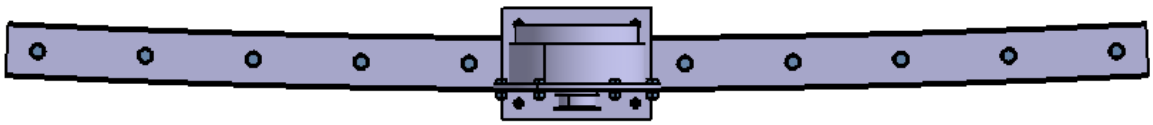

Figure 63: Top view of roller system defining motion of Beam Pipe

Both options are more or less relatively simple to realise. The solution with the rollers is more complex to produce, but the movement of Beam Pipe will have less resistance because of them, so it seems more convenient to use a rail system.

5.6. PSD passage

The last aspect to be resolved is the passage of the PSD detector. Each of the PSD modules weighs 500 kg, so the insert must carry a total weight of 1 500 kg. At this point, the smallest possible material budget must still be maintained. The use of metallic material will affect the measurement of the PSD detector, so a different material has to be chosen. For example, PEEK is a suitable material, but it will have to be designed to withstand the load. There were several variants (Figure 64) of what a PSD insert might look like, and an FEM analysis was done on one of them to see if it is possible.

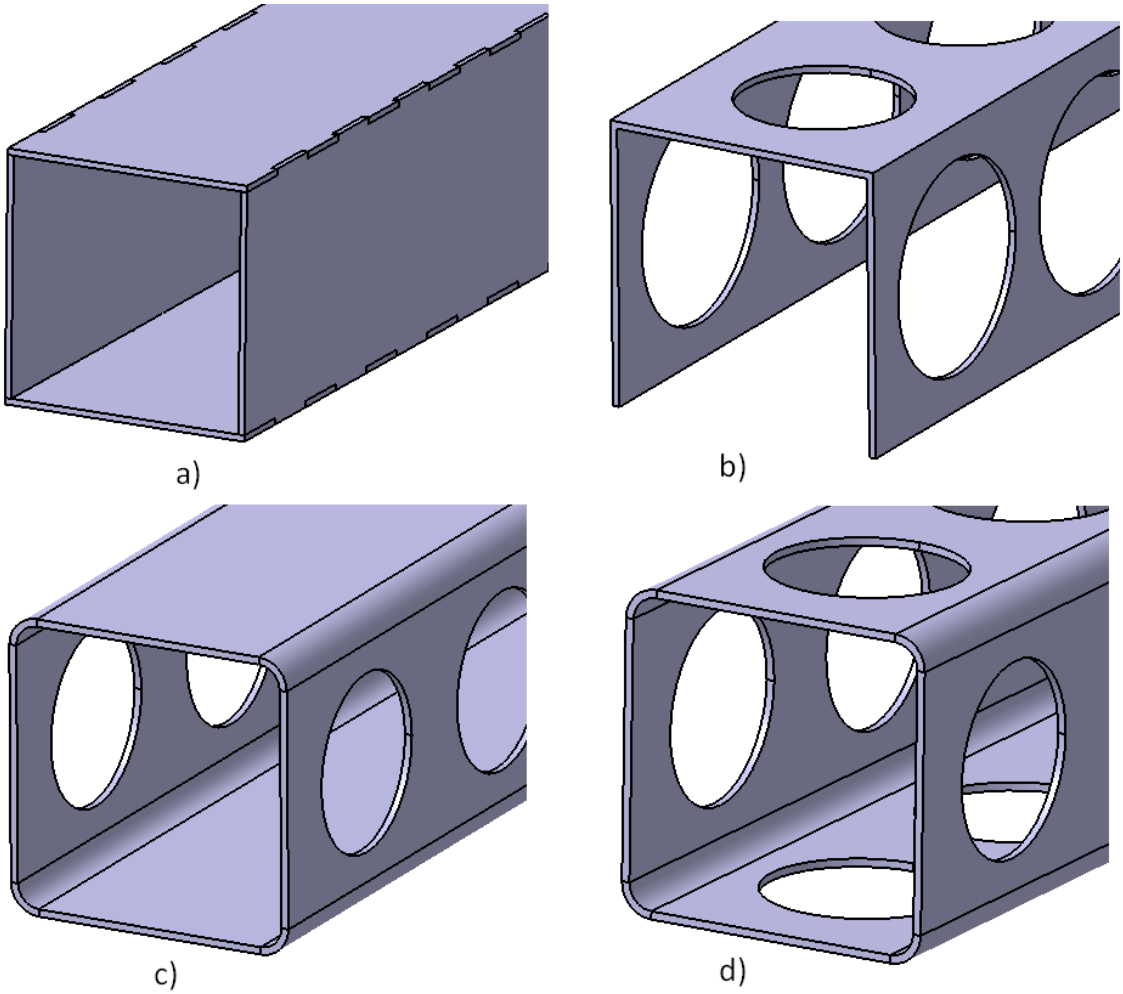

Figure 64: Variants of PSD insert passage part

5.6.1. FEM analysis

FEM analysis was done on option c) of Figure 64. In order to make the model as plausible as possible, a part (blue surface in Figure 65) has been created that represents the surrounding PSD modules and a plate representing the PSD modules above the passage. The wall thickness for the insert was chosen to be 5 mm. With this choice we have limited the dimensions of passage, which is therefore 190 x 190 mm.

The red surfaces on the PSD insert are connected to the blue surfaces via frictionless joint. These are surfaces representing the surrounding PSD modules and are set to be fixed.

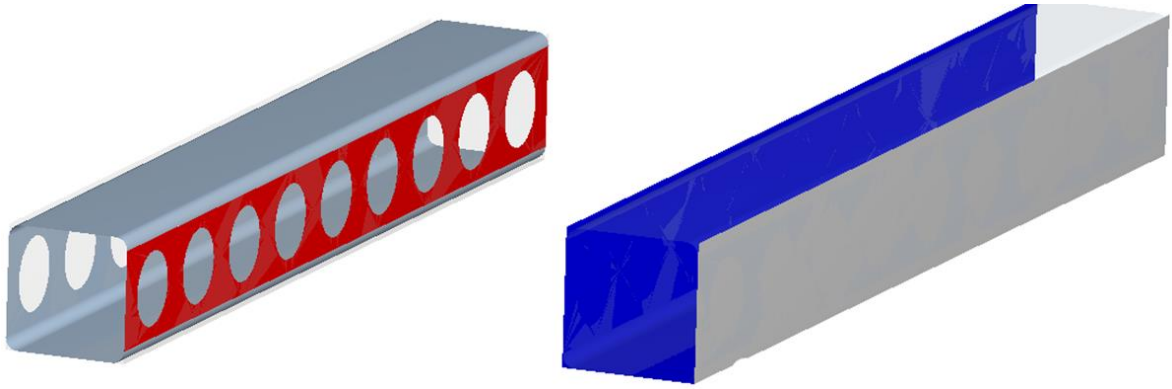

Figure 65: Surfaces with frictionless connection in Ansys model

The plate representing the PSD modules (green) is allowed to move in a vertical direction and is loaded with a force representing a mass of 1500 kg. The frictionless contact is set in the interface with the PSD insert (red surface).

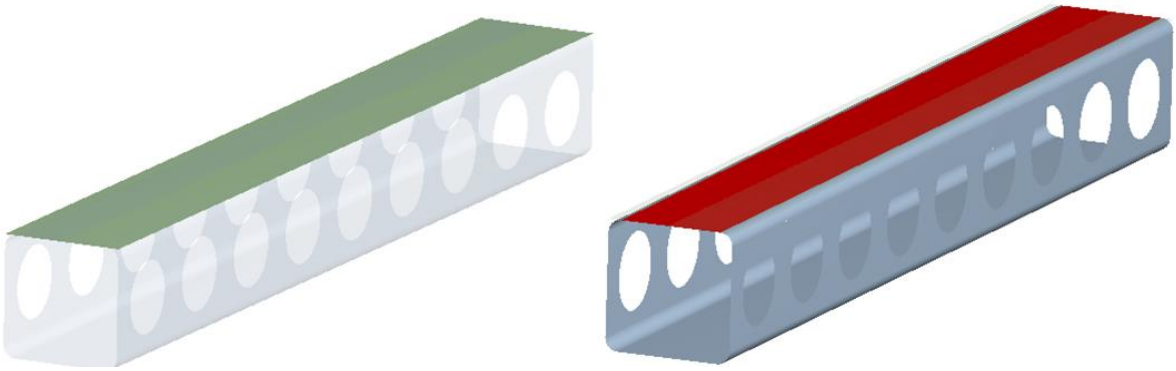

Figure 66: Surfaces with frictionless connection in Ansys model

The results (Figure 67 and Figure 68) show that the PSD insert deforms as expected. The maximum deformation is on the upper surface, which is 1.07 mm. With this deformation, the flange connection will not pass through, so the shape of the PSD insert will have to be altered, or the one depicted will have to be optimized. Due to stress, (when the maximum is 11.5 MPa), we are on the side of safety, because the R_m for PEEK is 115 MPa. So this piece could be used directly. If it further optimized, there will likely be even more material savings.

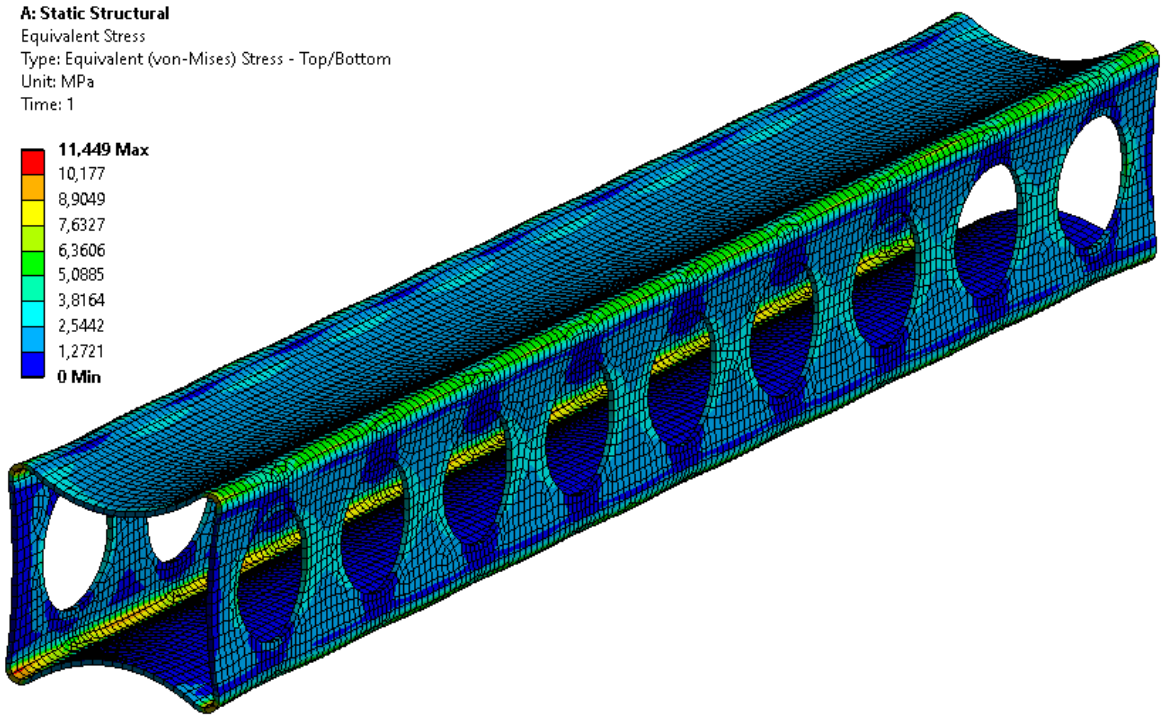

Figure 67: Equivalent (von-Mises) stress of PSD insert passage part

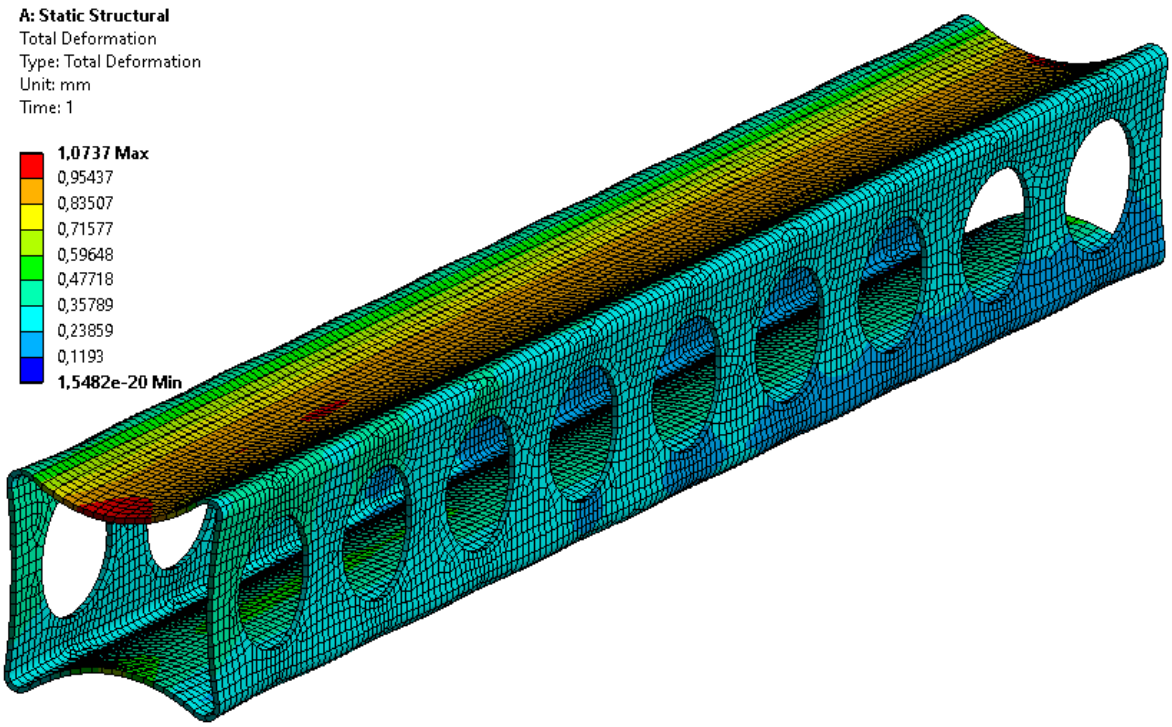

Figure 68: Total deformation of PSD insert passage part

5.7. Beam Pipe

As stated above, the whole Beam Pipe will be composed of several modules. Individual modules and types of connection can be combined in several ways. A schematic of possilble combinations is shown in Figure 69. What is needed now is to decide how many vacuum inputs will be needed, and adjust the lengths of each segment accordingly.

The Beam Pipe shown has a total of 4 inputs with ISO-KF flanges. The first piece has flange connections on both sides. One of the modules for vacuum input is the transition piece between the flange and slide-in connection. There are a total of 2 flange connections and 6 slide-in connections. The furthest position from the target is 19 000 mm. The total length of the pipe is 14 620 mm.

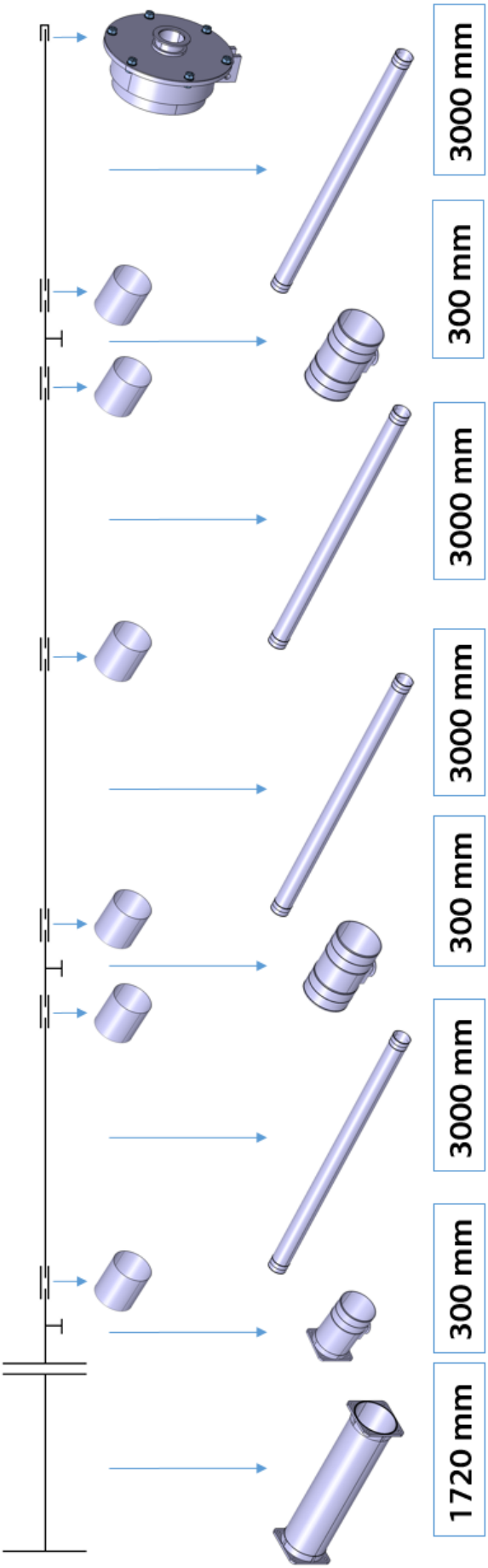

Figure 69: One of possible variants how Beam Pipe can look

6. Experiment

An experiment was performed to find out how the composite pipe, especially the matrix, will behave in a radiation environment. A short composite tube was made that was inserted between the glued PEEK flanges and closed by caps as shown in Figure 70. A hole was drilled in one cap and an ISO-KF flange was glued into it.

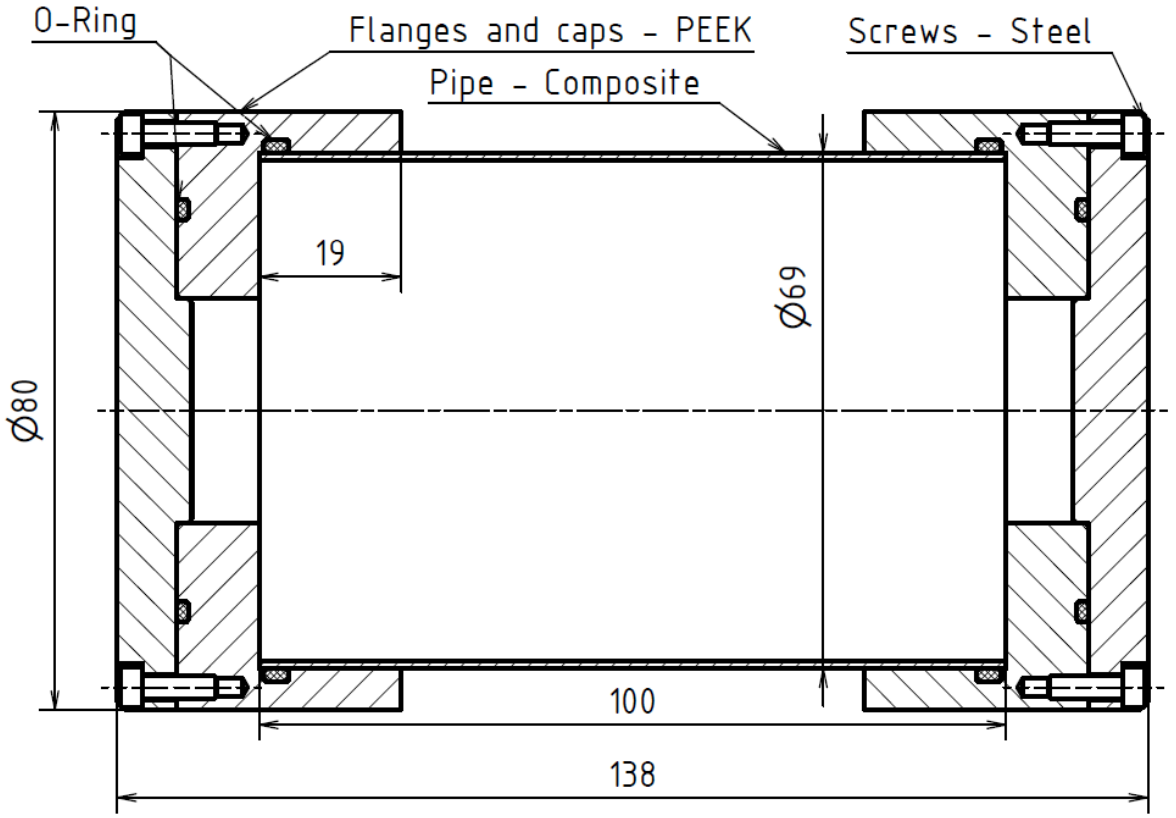

Figure 70: Section cut of part for experiment

A strain gauge (HBM 1-XY91-6/120) was glued to the surface of the composite pipe. After all the preparations, radiation was introduced. The fear was that the composite pipe might not be able to withstand it, a hole would be made in it, and fragments would destroy the vacuum pump. That didn't happen on the pipe, but the effect of the radiation showed up on the duct tape, which was damaged.

Measurement with strain gauges in radiation environments is a relatively unexplored topic. Before the measurements, it was not entirely clear what exactly was to be expected. Not much literature exists exploring this topic, and the determination of the behavior of strain gauges in a radiation environment was one of the aims of the experiment.

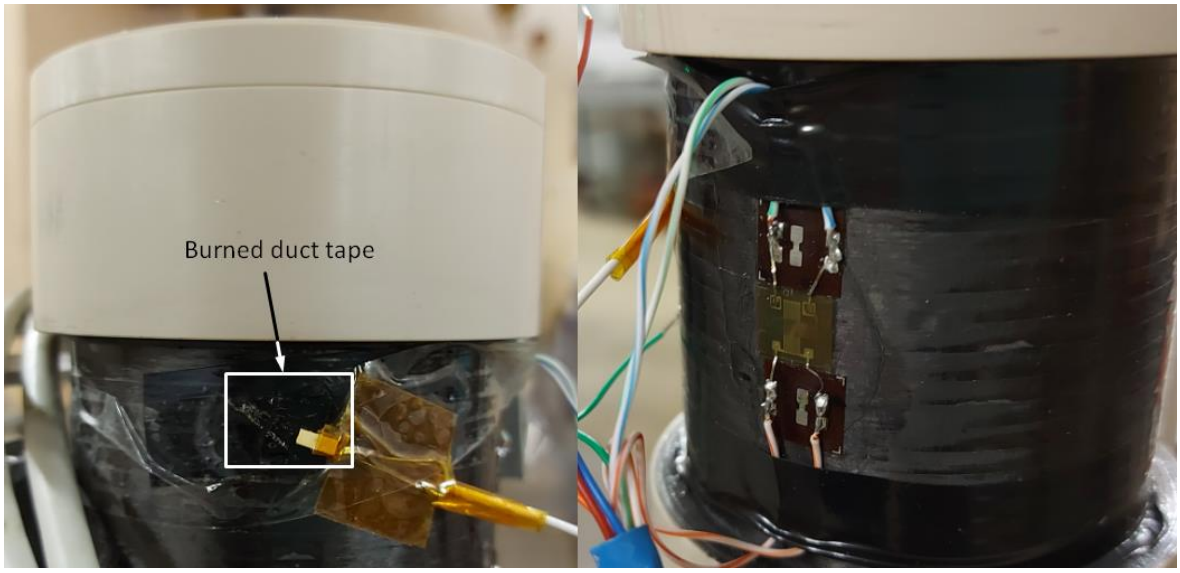

Figure 71: Burned duct tape in the left and strain gauge on composite pipe in the right

The measurement was made with a scanning frequency of 10 kHz. First there was data compression, because at a measurement time of roughly 190 minutes, a large amount of data was generated and the outputs were not meaningful. The output of the strain gauges is the difference in voltage relative to the supply voltage and this has been converted to deflection values per unit length using gauge factors for compressed data. Figure 71 shows the strain gauge on the composite pipe and in context with Figure 72, it is evident that coefficient a has to be used for strain in the axial direction and coefficient b has to be used for the radial strain.

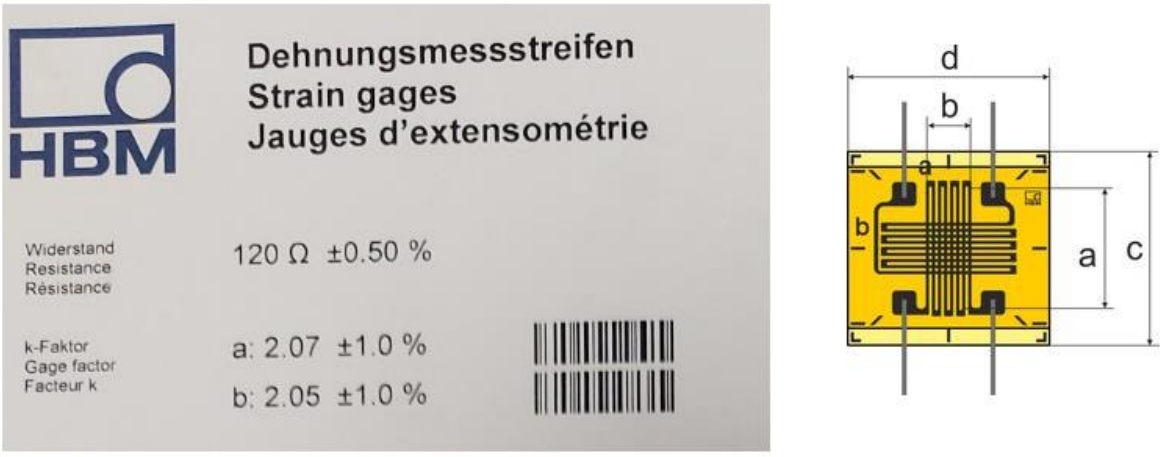

Figure 72: Gauge factor and schematic view on strain gauge [30]

The compressed data has been plotted. The plot in Figure 73 shows some important areas. The first is at a time of about 1 000 s, where a jump drop of the strain can be seen. The drop is caused by a vacuum where the pipe deforms after suction. The others are areas between 1500 – 3500 s and 4500 – 6 000 s. Significant background noise can be seen here that is caused by radiation. For better orientation, the data has been filtered from this noise and the strain values are much clearer in the plot which is shown in Figure 74.

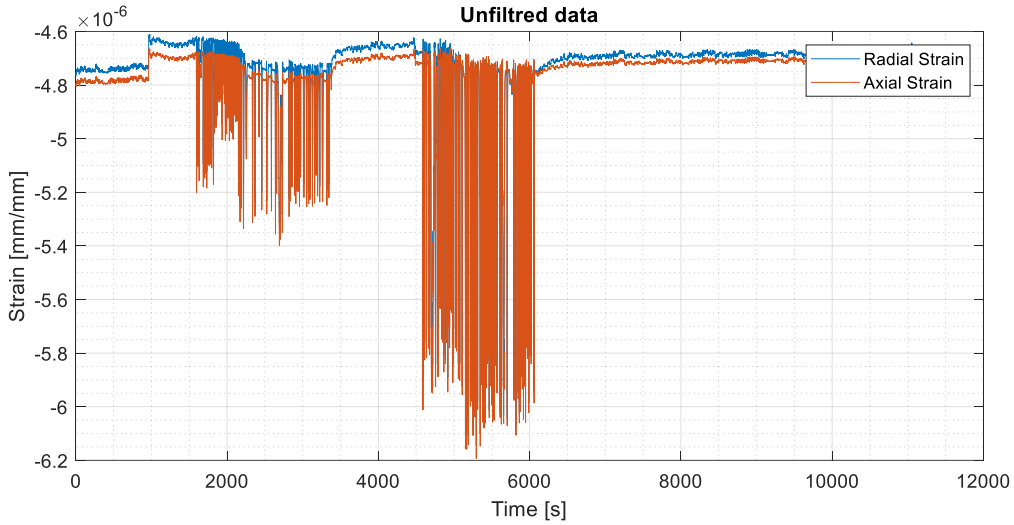

Figure 73: Unfiltered data of experiment

In time between 1500 and 4500 s, strain values begin to drop. Radiation causes the material to vaporize from the pipe into the space with vacuum. Vaporization also happens under normal conditions, but the radiation will significantly speed up the process. The released molecules impair the quality of the vacuum, which increases the pressure and causes the strain to decrease. At a time of 3500 - 4500 s, an increase in strains can be seen because the pipe is not exposed to radiation and the vacuum has stabilised again to a constant value. At the time when the pipe is exposed to radiation again, the process of vaporization is repeated and a re-decrease of strains is evident. After the radiation stops, the pressure stabilizes at a constant value. The maximum value of radial strain is $-4.640 \cdot 10^{-6}[mm/mm]$ and the maximum value of axial strain is $-4.705 \cdot 10^{-6}[mm/mm]$.

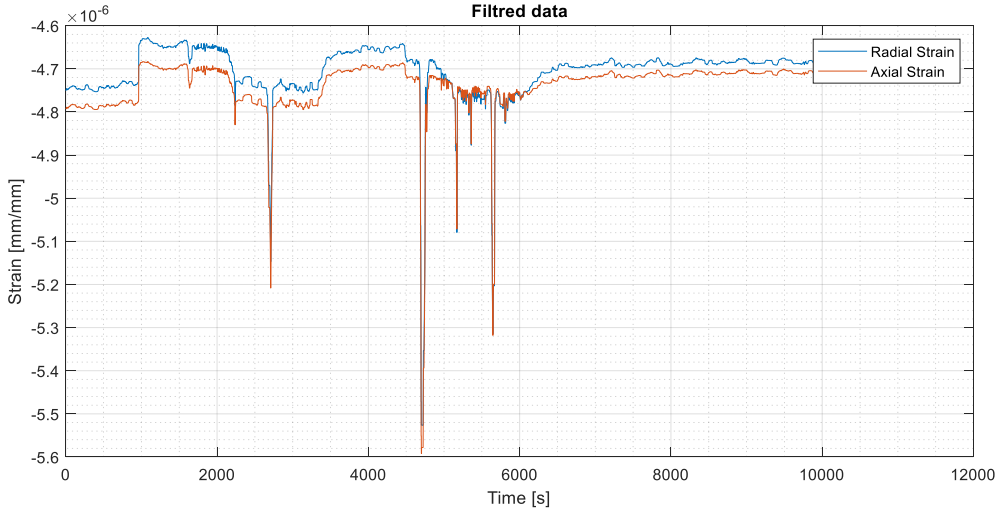

Figure 74: Filtered data of experiment

The goal of the FEM analysis is to achieve the same strain values that came out in the experiment. The flanges and caps have been simplified into one piece. A hole was made into one flange, and a fixed bond was applied to its surface, because the pipe was in fact attached to an ISO-KF flange glued into that hole. Pressure was applied on the inner walls

of the pipe, representing a vacuum. A cylindrical coordinate system was used to determine the strains on the pipe's surface in a direction perpendicular to the axis.

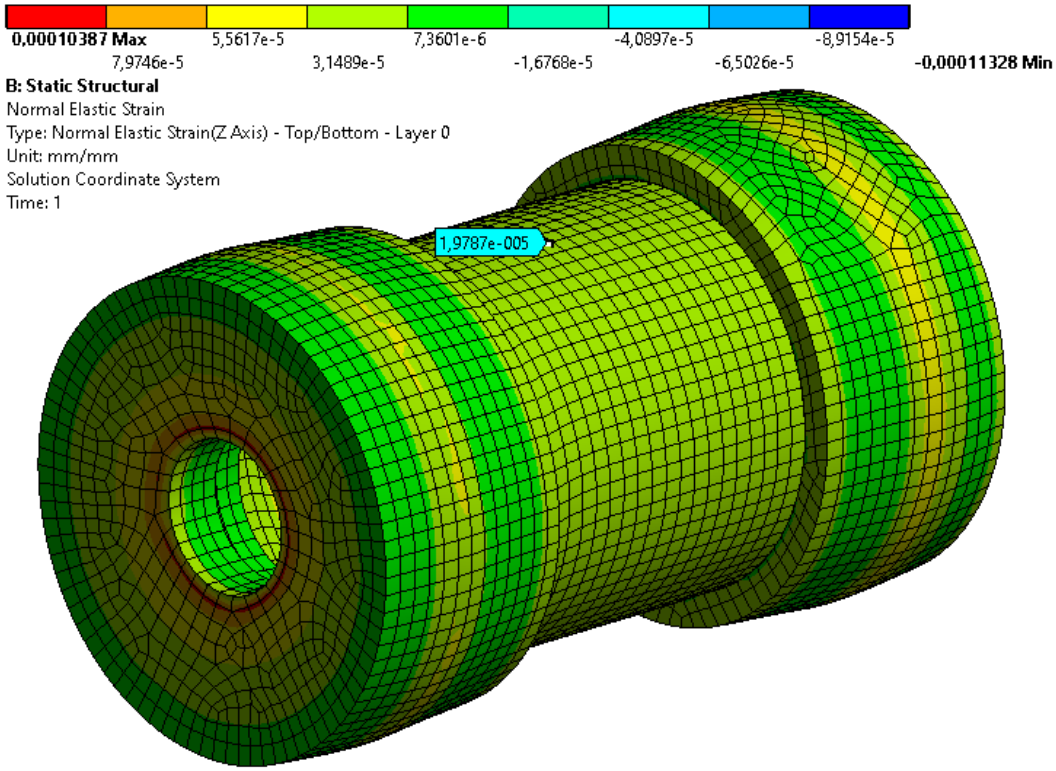

Figure 75: Results of axial strain from FEM analysis

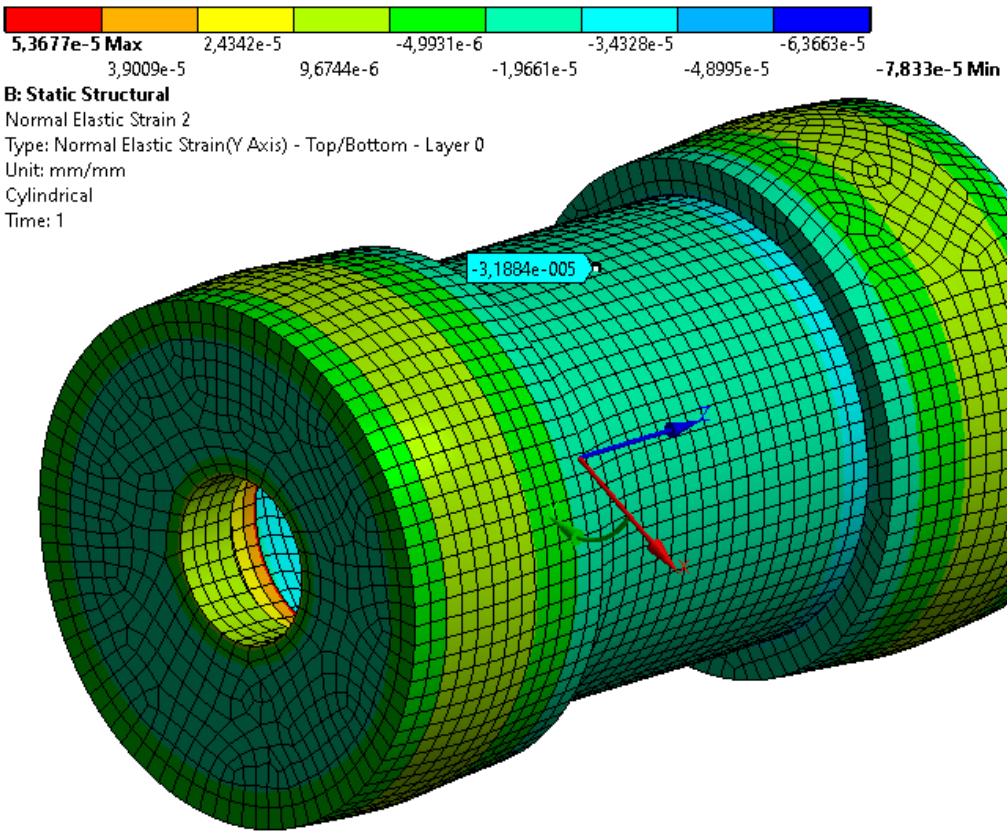

Figure 76: Results of radial strain from FEM analysis

7. Conclusion

The first stage of this thesis was the research carried out prior to the practical part. Its output was subsequently used further in the work. The research was made for composite materials and their manufacture. Information about vacuum was further presented, such as what a vacuum is, how we categorize it, and where it is used in real world applications. When the vacuum pumps were categorized, two pumps were selected, most likely to be used in the clean environment required by the FAIR accelerator. These two pumps were described in more detail. The final part of the research was the problematics of the O-rings.

The optimum number of vacuum inputs had to be designed first, so that the value of $1 \cdot 10^{-3}\ hPa$ was not exceeded. As achieving this quality of vacuum is not too difficult, a situation was considered where the vacuum input is only one in the end of the Beam Pipe. A vacuum pump with a pumping speed of $33\ l/s$ was chosen from the catalogue and the maximum pressure at the furthest point from the vacuum input was determined as $7.696 \cdot 10^{-4}\ hPa$, which is less than the required pressure and therefore one vacuum input for the required conditions is enough. But in reality, the pump speed would be lower, because there would be losses in the piping to the vacuum pump. Therefore, the location of the vacuum pumps will need to be known for a specific choice. Finally, a dependence between pressure and distance from vacuum input was made.

In choosing the O-rings, the material was chosen and the dimensions of the grooves calculated. The material most suitable for vacuum sealing is FPM (Fluorine Rubber - Viton). The dimensions of the vacuum sealing grooves were not given for all the dimensions of the O-rings, so they were calculated from the ratios of the groove areas and the cross-section of the O-ring.

While designing the Beam Pipe itself, it was first necessary to determine its basic dimensions. The length of the pipe was calculated based on the dimensions of the whole experiment. This length came out at $14920\ mm$, however it is not yet final as there is no determination as to what tilting mechanism will be used.

The diameter of the pipe is limited in the PSD passage, which is $200 \times 200\ mm$. In one of the PSD detector configurations, a part must be inserted part in the PSD passage that can support a mass of 1 500 kg. A PSD insert of PEEK has been designed to withstand this load, but reduced the passage to $190 \times 190\ mm$. This insert has also been subject to FEM analysis, which is in the Attachment (8). After establishing the dimensions of the passage, appropriate connections of pipes and wall thickness had to be proposed.

The wall thickness was designed to be 2 mm. Greater wall thickness would lead to undesirable material budget, and lower wall thickness could result in delamination. The wall thickness control was carried out using FEM analysis and comparing the inverse reserve factor. In the Attachments (6) and (7), FEM analysis of the pipe and connections are shown. At one point a demand existed that the tilt of the whole Beam Pipe would be controlled by a PSD detector that has its own drive. The tilting mechanism used a metal

bellow. At its extreme, a tilt of 2.5° and the overpressure produced a radial reaction of 3 500 N, so the metal bellow tended to return to a straight position. In the case where the PSD is in the furthest position, then, in controlling the tilt with the PSD detector, the Beam Pipe would have to overcome the bending moment from the reaction of 3 500 N and a distance of 12 m. Because the Beam Pipe will bend too much at this force, it could happen that the beam will not go through Beam Pipe due to the large deformation. Therefore, the maximum possible deformation for the individual wall thicknesses was determined. Thereafter, pipe deformations for a given load were detected using FEM analysis. A comparison of these results showed that it was not possible to control Beam Pipe's tilting in this way.

This was followed by the design of each module and their description. Two ways have been proposed for connecting individual modules. Flange connection and slide-in connection. The results of the FEM analysis (Attachments (6) and (7)) showed, that the flange connection has more stiffness, but it has a larger material budget. When choosing final connections, their combination still needs to be considered.

The Beam Pipe is at a 5 m height, so it needs to be supported somewhere. It is attached firmly to the tilting mechanism. At its end, before the beam dump there is a cap that allows air to be extracted out, while at the same time being mounted on a mechanism defining movement along the arc. Two types of this mechanisms were designed. One uses bushing and the other uses rollers - both are shown in the Attachments (2) and (3). Both mechanisms, if necessary, could also capture the axial force created by the pressure on the cap. The roller mechanism will have less resistance to movement, but has a larger material budget and its production is more sophisticated.

Two mechanisms using rollers have been proposed to support the pipe along its length. Rollers are proposed because currently, the location and motion of the detectors makes it impossible to determine the location where the support might be stationary. Either a support would have to be attached to one of the detectors and be adapted to move the Beam Pipe, or a position along the length of the pipe for a static support would have to be defined.

An entire model of the Beam Pipe was designed for one combination of flange and slide-in connections, which can however be changed. Four vacuum inlets are used, one is used for air extraction and three are used for measurement, possibly to be removed completely or sealed with a cap. A model is shown in Attachment (1).

Finally, an experiment was carried out. The test sample was a short composite tube with flanges made of PEEK. A strain gauge was glued to its surface, a vacuum was created and the pipe was exposed to radiation. The results showed that there is a lot of background noise in the radiation environment when measuring and increasing the pressure inside the pipe. This is due to vaporization, which is significantly accelerated by the effects of radiation. The last part of this work was an FEM analysis of the measured sample and a comparison of results. After setting the model and simulation, the results were found to be

different than those found by the experiment. The conclusion from the comparison of the results of the experiment to model of FEM analysis is that the strain values on the pipe's surface are different and the model will be subject to further work, however the model deforms as expected. Results of FEM analysis and processed data are contained in Attachments (4) and (5).

8. REFERENCE

[1] HÖHNE, C. a P. SENGER. *The CBM Physics Book*. 2011, , 863-925.

[2] FRIESE, V. a A. KOTYNIA. *Performance simulations of the CBM-STS with realistic material budget* [online]. In: . 2012 [cit. 2021-05-24]. Available on: https://repository.gsi.de/record/51962/files/PHN-NQM-EXP-28.pdf

[3] *Compressed Baryonic Matter (CBM)* [online]. [cit. 2021-05-28]. Available on: https://www.gsi.de/work/forschung/cbmnqm/cbm

[4] SENGER, Peter. Astrophysics in the Laboratory—The CBM Experiment at FAIR. *Particles*. 2020, **3**(2), 320-335. ISSN 2571-712X. Available on: doi:10.3390/particles3020024

[5] HEUSER, Johann M., L. BRAVINA, Y. FOKA a S. KABANA. Status of the CBM experiment. *EPJ Web of Conferences*. 2015, **95**. ISSN 2100-014X. Available on: doi:10.1051/epjconf/20159501006

[6] TURCSÁN, Tamás. *Developing of Nanostructured Polymer Composites* [online]. [cit. 2021-05-15]. Available on: http://doktori.bme.hu/bme_palyazat/2016/honlap/Turcsan_Tamas_gpk_en.html

[7] *History Of Composites* [online]. [cit. 2021-06-27]. Available on: http://compositeslab.com/composites-101/history-of-composites/

[8] NGO, Tri-Dung. Introduction to Composite Materials. *Composite and Nanocomposite Materials - From Knowledge to Industrial Applications*. IntechOpen, 2020. ISBN 978-1-78985-390-2. Available on: doi:10.5772/intechopen.91285

[9] KENDALL, K.N., C.D. RUDD, M.J. OWEN a V. MIDDLETON. Characterization of the resin transfer moulding process. *Composites Manufacturing*. 1992, **3**(4), 235-249. ISSN 09567143. Available on: doi:10.1016/0956-7143(92)90111-7

[10] BEDNÁR, Peter. *Návrh upravené technologie navíjení kompozitních trubek*. Brno, 2016. Diplomová práce. VUT v Brně.

[11] *The Pultrusion process* [online]. [cit. 2021-06-09]. Available on: https://www.strongwell.com/about/the-pultrusion-process/

[12] QUANJIN, Ma, M.R.M. REJAB, M.S. IDRIS, Bo ZHANG, M.N.M. MERZUKI a Nallapaneni Manoj KUMAR. Wireless technology applied in 3-axis filament winding machine control system using MIT app inventor. *IOP Conference Series: Materials Science and Engineering*. 2018, **469**. ISSN 1757-899X. Available on: doi:10.1088/1757-899X/469/1/012030

[13] QUANJIN, Ma, M R M REJAB, Jiang KAIGE, M S IDRIS a M N HARITH. Filament winding technique, experiment and simulation analysis on tubular structure. *IOP Conference Series: Materials Science and Engineering*. 2018, **342**. ISSN 1757-8981. Available on: doi:10.1088/1757-899X/342/1/012029

[14] VANDONI, G. CERN. *The basis of vacuum* [online]. [cit. 2021-07-27]. Available on: https://indico.cern.ch/event/264020/attachments/467855/648232/CERN-Basic-Vacuum-2012-lecture.pdf

[15] PFEIFFER VACUUM. *The Vacuum Technology Book: Volume II*. Asslar, Germany, 2013. Dostupné také z: www.pfeiffer-vacuum.com

[16] *Encyclopedia of physics*. 2nd ed. New York: VCH Publishers, 1991. ISBN 35-272-6954-1.

[17] PÁTÝ, Libor. *Vakuová technika*. Praha: České vysoké učení technické, 1990. ISBN 80-010-0216-0.

[18] SLAVÍČEK, Pavel, Vlasta ŠTĚPÁNOVÁ a Jakub KELAR. *Vakuová fyzika 1* [online]. Brno, 2016 [cit. 2021-07-27]. ISBN 978-80-210-8473-5. Available on: https://munispace.muni.cz/library/catalog/book/855

[19] *Everything you need to know about scroll pumps* [online]. 2019 [cit. 2021-07-17]. Available on: https://www.vacuumscienceworld.com/blog/everything-you-need-to-know-about-scroll-pumps

[20] LAMBERTZ, Peter. *Working with turbomolecular vacuum pumps* [online]. 2019 [cit. 2021-07-22]. Available on: https://www.vacuumscienceworld.com/blog/working-with-turbomulecular-vacuum-pumps

[21] *Flange Systems* [online]. Großlöbichau, Germany [cit. 2021-07-13]. Available on: https://www.vacom.de/en/products/standard-components/flange-systems/kf-components/290-en/products/standard-components/flange-systems

[22] KERSEVAN, Roberto. *Analytical and numerical tools for vacuum systems* [online]. 2007 [cit. 2021-06-27]. Available on: https://www.researchgate.net/publication/268373884_Analytical_and_numerical_tools_for_vacuum_systems

[23] O'HANLON, John F. *A User's Guide to Vacuum Technology*. Third Edition. Hoboken, New Jersey: A JOHN WILEY & SONS, INC., 2003.

[24] ADY, Marton a Roberto KERSEVAN. CERN. *MolFlow+ user guide*. 2014. Dostupné také z: https://molflow.web.cern.ch/sites/molflow.web.cern.ch/files/molflow_user_guide.pdf

[25] MOSHEY, E. A. *A Compilation of Outgassing Data on Vacuum Materials*. Princeton, NJ, 1982.

[26] WELCH, Kimo M. *The Pressure Profile in a Long Outgassing Vacuum Tube*. Stanford University, Stanford, California, 1972.

[27] DIMER S.R.O. *O-Rings*. 2012. Dostupné také z: www.dimer-group.com

[28] SALIX INTERNATIONAL. *O-kroužky: Katalog výrobků*. Zlín, Czech Republic. Dostupné také z: www.salixtesneni.cz

[29] KOLLARCZYK, Jan. *Design of a Tilting Mechanism of CBM experiment Beam Pipe*. Praha, 2021. Diploma thesis. Czech Technical University in Prague, Faculty of Mechanical Engineering.

[30] *XY T Rosettes with 2 Measuring Grids for Analyzing Biaxial Stress States with Known Principal Directions* [online]. [cit. 2021-07-27]. Available on: https://www.hbm.com/en/3443/xy-t-rosettes-with-measuring-grids-for-analyzing-biaxial-stress

LIST OF FIGURES

Figure 1: Overview of FAIR (up) and CBM Experiment (down) [4] [5] 4
Figure 2: Structure of long fibre reinforced composite material in case of same oriented (up) and normal to each oriented (down) fibre reinforcement [6] 5
Figure 3: Hand lay-up process [8] 7
Figure 4: The schematic view of the resin infusion process [8] 7
Figure 5: The schematic view of compression moulding process [8] 8
Figure 6: Alternative process of compression moulding [10] 8
Figure 7: The schematic view of pultrusion process [11] 9
Figure 8: The schematic view of filament winding process [12] 10
Figure 9: Filament winding process generation: (a) first passage, (b) first circuit, (c) third passage, (d) double fibre +ϕ/-ϕ fibre orientation [13] 10
Figure 10: Construction and functional principle of scroll vacuum pump [18] 13
Figure 11: Construction types of turbomolecular vacuum pumps – horizontal arrangement in the left and vertical arrangement in the right. 1 – rotor, 2 – inlet, 3 – outlet [18] 14
Figure 12: ISO-KF flange assembly [21] 16
Figure 13: ISO-K flange [21] 16
Figure 14: ISO-F flange 17
Figure 15: ISO-CF flange [21] 17
Figure 16: Detail of sealing of ISO-CF connection [21] 18
Figure 17: The schematic view of vacuum conductance 18
Figure 18: Pressure profile (red) in long tube 19
Figure 19: Potential sources of gases in vacuum systems [23] 20
Figure 20: Particle trajectories in the left and visualized particles escaping from the system in the right [24] 21
Figure 21: MolFlow+ simulation result [24] 22
Figure 22: Dependence of pressure on distance from vacuum input 24
Figure 23: Section cut through O-ring [27] 25
Figure 24: Material of O-rings [27] 25
Figure 25: Dependence between O-ring hardness and pressure [28]2 26
Figure 26: Dimensions of groove for O-ring 27
Figure 27: Overview of Beam Pipe 30
Figure 28: Configurations of PSD detector 30
Figure 29: The schematic view of tilted Beam Pipe with deformed and undeformed Pipe 32
Figure 30: Difference in rotation with vacuum load 33
Figure 31: Difference in rotation without vacuum load 33
Figure 32: Slide-in connection 34
Figure 33: Section cut of slide-in connection 35
Figure 34: Disassembled slide-in connection 35
Figure 35: Position of section cuts 36
Figure 36: Section cut C-C 36
Figure 37: Section cut D-D with detail of groove for O-ring 37
Figure 38: Disassembled flange connection 37
Figure 39: Flange connection 38
Figure 40: Total deformation of Slide-in connection 39
Figure 41: Inverse reserve factor of Slide-in connection 39
Figure 42: Total deformation of Flange connection 39
Figure 43: Inverse reserve factor of Flange connection 39
Figure 44: First piece of Beam Pipe 40
Figure 45: Disassembled first piece of Beam Pipe 40
Figure 46: Transition piece of Beam Pipe 41
Figure 47: Disassembled transition piece of Beam Pipe 41
Figure 48: Long part of Beam Pipe 42

Figure 49: Detail of end of long Beam Pipe part 42
Figure 50: Beam Pipe's cap with vacuum input 43
Figure 51: Disassembled Beam Pipe's cap with vacuum input 43
Figure 52: Section cut of Beam Pipe's cap 44
Figure 53: Vacuum input with cylindrical outlet on pipe 45
Figure 54: Vacuum input with extra part 45
Figure 55: Concepts for Beam Pipe's support 46
Figure 56: Flange connection modification for support with rollers 46
Figure 57: Slide-in connection modification for support with rollers 47
Figure 58: The schematic view of motion of Beam Pipe 47
Figure 59: End cap with controlling mechanism 48
Figure 60: Arc groove defining motion of Beam Pipe 49
Figure 61: Roller system defining motion of Beam Pipe 49
Figure 62: Section cut of roller system defining motion of Beam Pipe 50
Figure 63: Top view of roller system defining motion of Beam Pipe 50
Figure 64: Variants of PSD insert passage part 51
Figure 65: Surfaces with frictionless connection in Ansys model 51
Figure 66: Surfaces with frictionless connection in Ansys model 52
Figure 67: Equivalent (von-Mises) stress of PSD insert passage part 52
Figure 68: Total deformation of PSD insert passage part 53
Figure 69: One of possible variants how Beam Pipe can look 54
Figure 70: Section cut of part for experiment 55
Figure 71: Burned duct tape in the left and strain gauge on composite pipe in the right 56
Figure 72: Gauge factor and schematic view on strain gauge [30] 56
Figure 73: Unfiltered data of experiment 57
Figure 74: Filtered data of experiment 57
Figure 75: Results of axial strain from FEM analysis 58
Figure 76: Results of radial strain from FEM analysis 58

LIST OF TABLES

Table 1: Vacuum categories according to vacuum quality 11
Table 2: Dimensions of groove for O-rings for vacuum [27] 26
Table 3: Dependce of diameter d_1 tolerances to its main dimension [28] 26
Table 4: Results of groove for O-ring dimensions dependent do d_2 28
Table 5: Results of allowed differences and results of difference in rotation from Ansys 32

LIST OF ATTACHMENTS

Attachment (1)	CAD model:	"Beam_Pipe.stp"
Attachment (2)	CAD model:	"End_support_bushing.stp"
Attachment (3)	CAD model:	"End_support_rollers.stp"
Attachment (4)	Matlab Data:	"processed_experiment.rar"
Attachment (5)	Ansys Analysis:	"fem_experiment.wbpz"
Attachment (6)	Ansys Analysis:	"fem_slidein.rar"
Attachment (7)	Ansys Analysis:	"fem_flange.rar"
Attachment (8)	Ansys Analysis:	"fem_psd_passage.rar"